Biochimica et Biophysica Acta 1861 (2017) 3129–3143

Contents lists available at ScienceDirect

Biochimica et Biophysica Acta

journal homepage: www.elsevier.com/locate/bbagen

Membrane damage by betulinic acid provides insights into cellular aging

Waleska K. Martins [a,b], Andreza B. Gomide [c,d], Érico T. Costa [e], Helena C. Junqueira [a], Beatriz S. Stolf [f], Rosangela Itri [c], Maurício S. Baptista [a,*]

[a] Instituto de Química, Universidade de São Paulo, Brazil
[b] Universidade de Santo Amaro, Brazil
[c] Instituto de Física, Universidade de São Paulo, Brazil
[d] Centro Universitário Padre Anchieta, Brazil
[e] Ludwig Institute for Cancer Research (LICR) at Centro de Oncologia Molecular, Hospital Sírio Libanês, São Paulo, Brazil
[f] Instituto de Ciências Biomédicas, Universidade de São Paulo, Brazil

ARTICLE INFO

Article history:
Received 9 June 2016
Received in revised form 19 October 2016
Accepted 19 October 2016
Available online 20 October 2016

Keywords:
Membrane biophysics
Autophagy impairment
Lipofuscinogenesis
Redox misbalance
Senescence, Mitochondrial-lysosomal axis theory of aging

ABSTRACT

Background: Cell senescence is a process of central importance to the understanding of aging as well as to the development of new drugs. It is related with genomic instability, which has been shown to occur in the presence of autophagy deficiency. Yet, the mechanism that triggers genomic instability and senescence from a condition of autophagy deficiency remains unknown. By analyzing the consequences of treating human keratinocytes (HaCaT) with the pentacyclic triterpenoid Betulinic Acid (BA) we were able to propose that cell senescence can develop as a response to parallel damage in the membranes of mitochondria and lysosome.
Methods: We performed biochemical, immunocytochemical and cytometric assays after challenging HaCaT cells with BA. We also evaluated membrane leakage induced by BA in liposomes and giant unilamellar vesicles.
Results: By destabilizing lipid bilayers of mitochondria and lysosomes, BA triggers the misbalance in the mitochondrial-lysosomal axis leading to perceived autophagy impairment, lipofuscinogenesis, genomic instability and cell senescence. The progressive accumulation of mitochondria and lipofuscin, which comes from imperfect mitophagy triggered by BA, provides a continuous source of reactive species further damaging lysosomes and leading to cell aging.
Conclusions: This work reveals that the initial trigger of cell senescence can be the physical damage in the membranes of lysosomes and mitochondria.
General significance: This concept will help in the search of new drugs that act as senescence-inductors. BA is under evaluation as chemotherapeutic agent against several types of tumors and induction of cell senescence should be considered as one of its main mechanisms of action.

1. Introduction

Cellular aging is characterized by a progressive loss of physiological integrity, resulting in gradual functional decline [1]. There are several cellular and molecular hallmarks of cell aging such as genomic instability, telomere attrition, senescence, low proteostasis and altered intercellular communication [1].

Cellular senescence implicates in a persistently growth-arrest phenotype, being the common output response to different stressors that activate DNA damage response (DDR) and eventually the p53/p21 and p16 axes [2]. Shortened telomeres can be caused by successive DNA replications, and activate DDR leading to *replicative senescence* [2–4]. Other possible cause of shortened telomeres is the formation of single-stranded overhangs at the end of telomeres triggered by oxidative stress [4]. As reported, the telomere shortening associated with replicative aging was modulated according to the amount of oxidative stress [4]. DDR system can also be activated in telomere-independent modes, such as in stress-induced premature senescence (SIPS) or in oncogene-induced senescence (OIS) [5].

Autophagy is also related to senescence, but its actual role seems to depend on the cellular context and on the experimental settings [6]. Some reports showed the contribution of autophagy disruption to age-related phenotype as reviewed by Rubinsztein and co-workers [7].

Abbreviations: AAU, Autophagy Arbitrary Units; BA, Betulinic Acid; Cathepsin B, CTSB; CQ, Chloroquine; COXIV, cytochrome *c* oxidase subunit iv; CVS, Crystal Violet Staining; DMEM, Dulbecco's modified Eagle's medium; DDR, DNA damage response; FBS, fetal bovine serum; GAPDH, Glyceraldehyde-3-Phosphate Dehydrogenase; LMP, Lysosomal membrane permeabilization; MTT, 3-(4,5-Dimethylthiazol-2-yl)-2,5-Diphenyltetrazolium Bromide; NR, Neutral Red; OIS, oncogene-induced senescence; POPC, 1-palmitoyl,2-oleoyl-sn-glycero-3-phosphocholine; DPPE, 1,2-Dipalmitoyl-sn-glycero-3-phosphoethanolamine; SIPS, stress-induced premature senescence; Mitochondrial membrane potential, $\Delta\Psi m$.

* Corresponding author at: Department of Biochemistry, Sao Paulo University, Av. Prof. Lineu Prestes 748 room 1262. CEP 05508-000, Sao Paulo, Brazil.
E-mail address: baptista@iq.usp.br (M.S. Baptista).

http://dx.doi.org/10.1016/j.bbagen.2016.10.018
0304-4165/

A phenomenological link between the decrease in metabolic homeostasis and aging has been proposed by Brunk and colleagues [8,9]. Several data support the mitochondrial-lysosomal axis theory of aging, since age-related alterations in mitochondria and lysosome amplify each other, inducing profound dysfunction of several cellular processes [10]. However, the molecular events that trigger the loss in mitochondrial-lysosomal homeostatic axis are still object of conjecture [11].

In here, we employed human skin keratinocytes (HaCaT) to test the hypothesis that the biophysical disruption in lysosomal and mitochondrial membranes act as the initial trigger of cell senescence. HaCaT is a cell line whose differentiation strictly depends on autophagy [12], and consequently, it is possible to directly detect endogenous LC3 lipidated form (LC3-II), avoiding artifacts that may occur when employing transfection and transgenesis strategies. Betulinic Acid (BA) is a pentacyclic triterpenoid whose molecular structure reminds that of cholesterol, allowing it to strongly interact with membranes, but contrarily to cholesterol, it causes an important disruption in the membrane's structure [15]. BA has several pharmacological applications, including the treatment of aggressive cancers such as non-responsive melanomas [13]. Several mechanisms of BA action on mammalian cells have been described, including induction of apoptosis and modulation of autophagy [14–18]. Nevertheless, senescence has never before been linked to BA.

2. Material and methods

2.1. Cell lines and cell culture

Human skin keratinocyte cell line (HaCaT) [19] was cultured in DMEM (Sigma-Aldrich) supplemented with 10% (*v*/v) fetal bovine serum (FBS), 100 U/mL of penicillin, and 100 pg/mL of streptomycin in a 37 °C incubator at a moist atmosphere of 5% carbon dioxide.

2.2. The time course of HaCaT cells treatment with BA

Right after a 24 h-treatment with BA (Sigma-Aldrich) at 20 μM (i. e. IC_{50}) and 0.25% (*v*/v) Dimethyl sulfoxide (DMSO, Sigma-Aldrich) [16], referred here as T1, HaCaT cells were washed and incubated in freshed medium supplemented with 10% (*v*/v) FBS. Thus, after BA treatment removal, HaCaT cells were chased for periods T2, T3, T4 and T5 that correspond to a long-term cellular response at 24 h, 48 h, 96 h and 120 h, respectively.

2.3. Determination of lysosomal accumulation by cytochemical-staining

BA was dissolved in DMSO (4 mg/mL) and diluted to 20 μM in DMEM (Sigma-Aldrich) supplemented with 1% (*v*/v) FBS, 100 U/mL of penicillin, and 100 pg/mL of streptomycin. 24 h after seeding, we treated HaCaT with BA (20 μM) for 24 h in a 37 °C incubator at a moist atmosphere of 5% carbon dioxide. After indicative period of times, cells were stained with 30 μg/mL Neutral Red (NR, Sigma-Aldrich) at 37 °C for 2 h and washed twice with PBS. Next, NR was eluted with a 1% (*v*/v) alcoholic-based acetic acid fixing solution for 10 min at room temperature and measured at 540 nm using the Infinite M-200 Tecan microplate reader (Männedorf, Switzerland), with a wavelength correction set at 800 nm for subtraction of backgrounds. Cell survival rates were normalized to the absorbance values of untreated cells and represented as percentage.

Lysosomal accumulation was characterized by the uptake of lysosomotropic dye NR as described above and visualized under an inverted microscope for transmitted light (Zeiss™ Axiovert 200) equipped with an C-APOCHROMAT 40×/1.20 W Corr M27 objective (Zeiss™) and imaged using Image J Software (National Institutes of Health, Bethesda). Alternatively, to monitor cell death associated with accumulation of acidic vacuoles we performed combined staining using Acridine Orange (AO) and Propidium Iodide (PI). After washing, we immediately analyzed live-cells under microscope for epifluorescence (Zeiss™ Axiovert 200) equipped with an C-APOCHROMAT 40×/1.20 W Corr M27 objective (Zeiss™) using the filter set 09 (Zeiss™) that provides an excitation band pass (BP) of 450–490 nm with emission long pass (LP) of 515 nm.

2.4. Cell survival assays

Cell viability was evaluated by usual chemical staining methods, such as MTT and CVS (Crystal Violet Staining), as well as by clonogenic assay (see below). MTT and CVS were performed as described [15]. Briefly, in each sample we added 0.2 mL of DMEM supplemented with 50 μg/mL 3-(4,5-Dimethylthiazol-2-yl)-2,5-Diphenyltetrazolium Bromide (MTT, Sigma-Aldrich), 1% (*v*/v) FBS, 100 U/mL of penicillin, and 100 pg/mL of streptomycin and incubated at 37 °C for 2 h. At the end of the incubation period, the DMEM with MTT was removed and 0.1 mL DMSO (Sigma-Aldrich) was added. The plate was shaken and absorbance values were read at 550 nm (Infinite M-200 Tecan microplate reader, Switzerland). For the CVS assay, NR-labeled wells were washed twice with distilled water and stained with 0.02% (*w*/*v*) Crystal Violet (CV, Sigma-Aldrich) for 5 min at room temperature. After washing with distilled water, CV was eluted by 50% (*v*/v) ethanol containing 0.1 M sodium citrate, and absorbance was read at 585 nm. For both assays cell survival rates were normalized to the absorbance values of untreated cells.

2.5. AAU calculation

We analyzed the correlation between the lysosomotropic vacuolization and cell viability according to a recent strategy of quantifying autophagy by arbitrary units (AAU). To calculate AAU, the NRU survival rate was normalized to the mean of the MTT and CVS survival rates according to the function w (x, y, z):

$$w = \frac{1}{2}\left[\left(\frac{x}{y}\right) + \left(\frac{x}{z}\right)\right]$$

where x, y, and z were the survival rates measured by NRU, CVS and MTT assays, respectively. Next, the propagated error, σ_w, of the function w (x, y, z) was determined according to formula below:

$$\sigma_w = w * \sqrt{\left(\frac{\sigma_x}{x}\right)^2 + \left(\frac{\sigma_y}{y}\right)^2 + \left(\frac{\sigma_z}{z}\right)^2}$$

where the σ_x, σ_y and σ_z are the error deviations calculated for NRU, CVS and MTT, respectively.

2.6. GUVs analysis

The GUVs were prepared according to electroformation method. Briefly, we spread 20 μL of a chloroform solution containing 2 mg/mL POPC (1-palmitoyl,2-oleoyl-sn-glycero-3-phosphocholine) and 0.2% (*w*/*v*) of the total lipid Rhodamine-DPPE (1,2-Dipalmitoyl-sn-glycero-3-phosphoethanolamine) on the surfaces of two conductive glasses coated with Fluor Tin Oxide. Next, we placed them with their conductive sides facing each other and separated by a 2 mm thick Teflon frame. This electro-swelling chamber was filled with 0.2 M sucrose solution, and was connected to an alternating electric field of 2 V with a 10 Hz frequency for 2 h as described [20]. The vesicle suspension was removed from the chamber and diluted into a glucose solution (0.2 M) containing BA (100 μM). The osmolarity of the sucrose and glucose solutions was measured with a Gonotec 030 cryoscopic osmometer (Osmomat®) before use, and they were carefully matched to avoid osmotic pressure effects. Vesicles were immediately placed on the observation chamber. Due to the differences in density between sucrose and

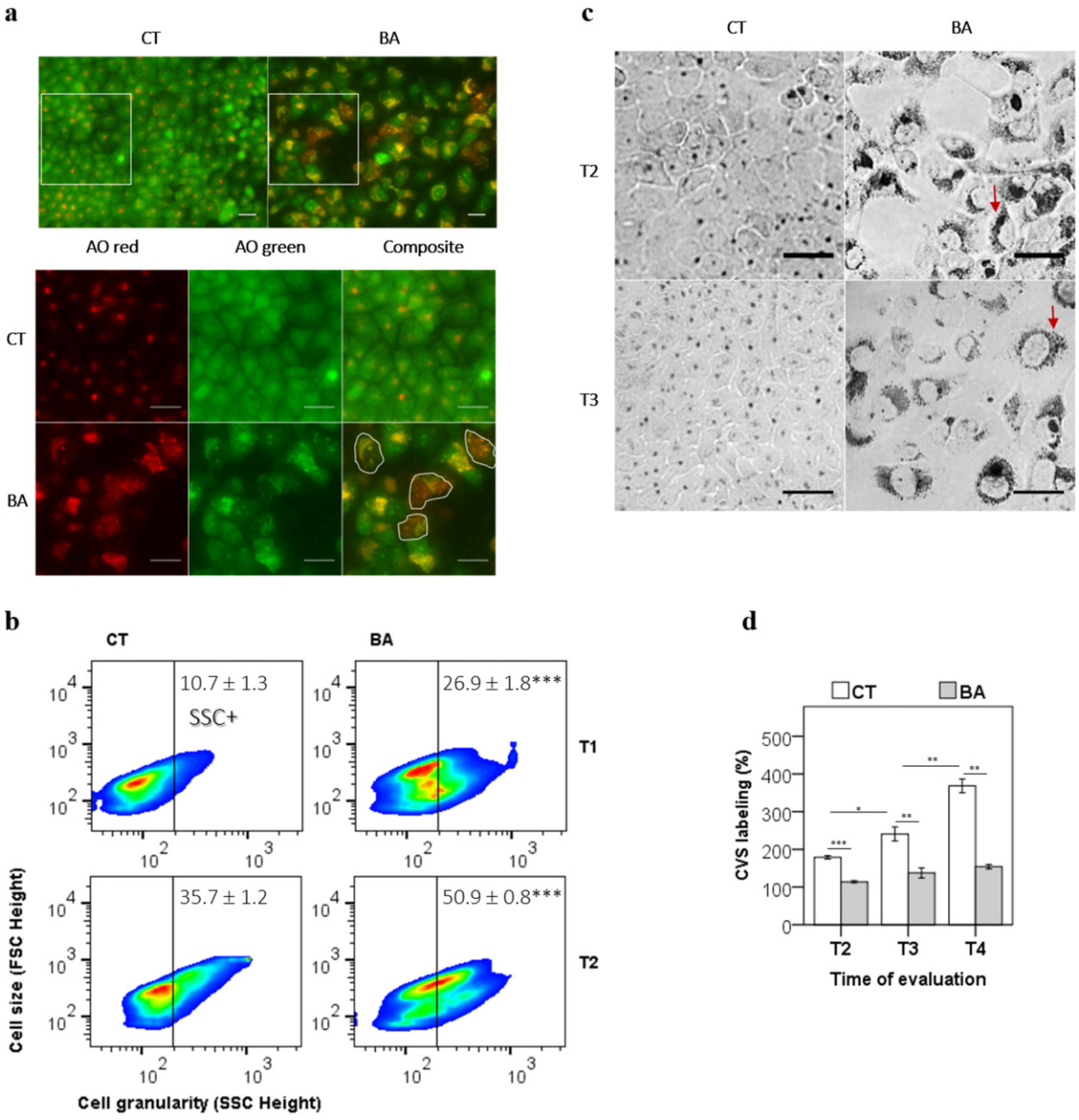

Fig. 1. BA treatment causes cell death and/or growth arrest with inhibition of autophagy and accumulation of acidic vacuoles. (a) Right after BA treatment, micrographs of treated cells following Propidium Iodide (PI) and Acridine Orange (AO) staining. In bottom panel, zoom micrographs of image areas encircled by a dashed line (top panel). (b) At T1 and T2, scatter-plots of cell subpopulations gated as function of cell size (FSC Height) and granularity (SSC Height). Right quadrants show the frequency of vacuolated cells (SSC^+). (c) At T2 and T3 micrographs of treated cells following Neutral Red (NR) uptake. Red arrows show increase in NR uptake within acidic vacuoles. (d) Following indicative times (T2 to T4) the proliferation rates quantified by Crystal Violet Staining (CVS) assay compared to values observed for CT at T1 and expressed as percentage. For Panel b and d mean ± standard error of three independent experiments are shown. The significance of differences after BA in comparison to control (CT) was indicated as $^*P < 0.05$; $^{**}P < 0.01$; $^{***}P < 0.0001$. Scales bar in (a) and (c) are 20 μm.

Table 1
Survival rates of HaCaT evaluated at T1, right after a 24 h-treatment with 0.25% (v/v) DMSO (CT) and 20 μM Betulinic Acid (BA), and after following the vital cells at longer-time course: at 24 h (T2); 48 h (T3); 96 h (T4) and 120 h (T5).

Time	Cellular viability			Cellular density			Cellular viability			Lysosomal content		
	NRU assay			**CVS assay**			**MTT assay**			**(AAU)**		
	CT	BA	P	CT	BA	P	CT	BA	P	CT	BA	P
T1	101 ± 0.6	65 ± 2.2	<0.001	119 ± 5.8	75 ± 2.2	<0.001	102 ± 1.8	50 ± 3.2	<0.001	0.9 ± 0.05	1.1 ± 0.09	0.002
T2	99 ± 0.7	76 ± 1.4	<0.001	100 ± 2.4	48 ± 0.8	<0.001	100 ± 1.5	35 ± 1.8	<0.001	1.0 ± 0.03	1.9 ± 0.11	<0.001
T3	98 ± 1.0	82 ± 3.6	<0.001	100 ± 4.9	42 ± 3.9	<0.001	100 ± 2.2	30 ± 1.3	<0.001	1.0 ± 0.05	2.3 ± 0.26	<0.001
T4	101 ± 1.9	80 ± 2.7	<0.001	100 ± 5.0	55 ± 2.0	<0.001	100 ± 1.0	62 ± 1.2	<0.001	1.0 ± 0.05	1.4 ± 0.07	<0.001
T5	105 ± 2.6	93 ± 2.7	<0.001	100 ± 3.7	64 ± 2.9	<0.001	104 ± 1.7	53 ± 0.9	<0.001	1.0 ± 0.05	1.6 ± 0.09	<0.001

Mean ± standard error of three independent experiments.

glucose solutions, vesicles were stabilized by gravity at the bottom of the observation chamber. Under inverted microscope Axiovert 200 (Zeiss™) vesicles were observed in phase contrast Plan Neo-Fluar 63× Ph2 objective (NA 0.75) and fluorescence (103 W Hg lamp, HXP 120, Kubler, Carl Zeiss, Jena, Germany) modes. Images were recorded using an AxioCam HSm digital camera (Zeiss™).

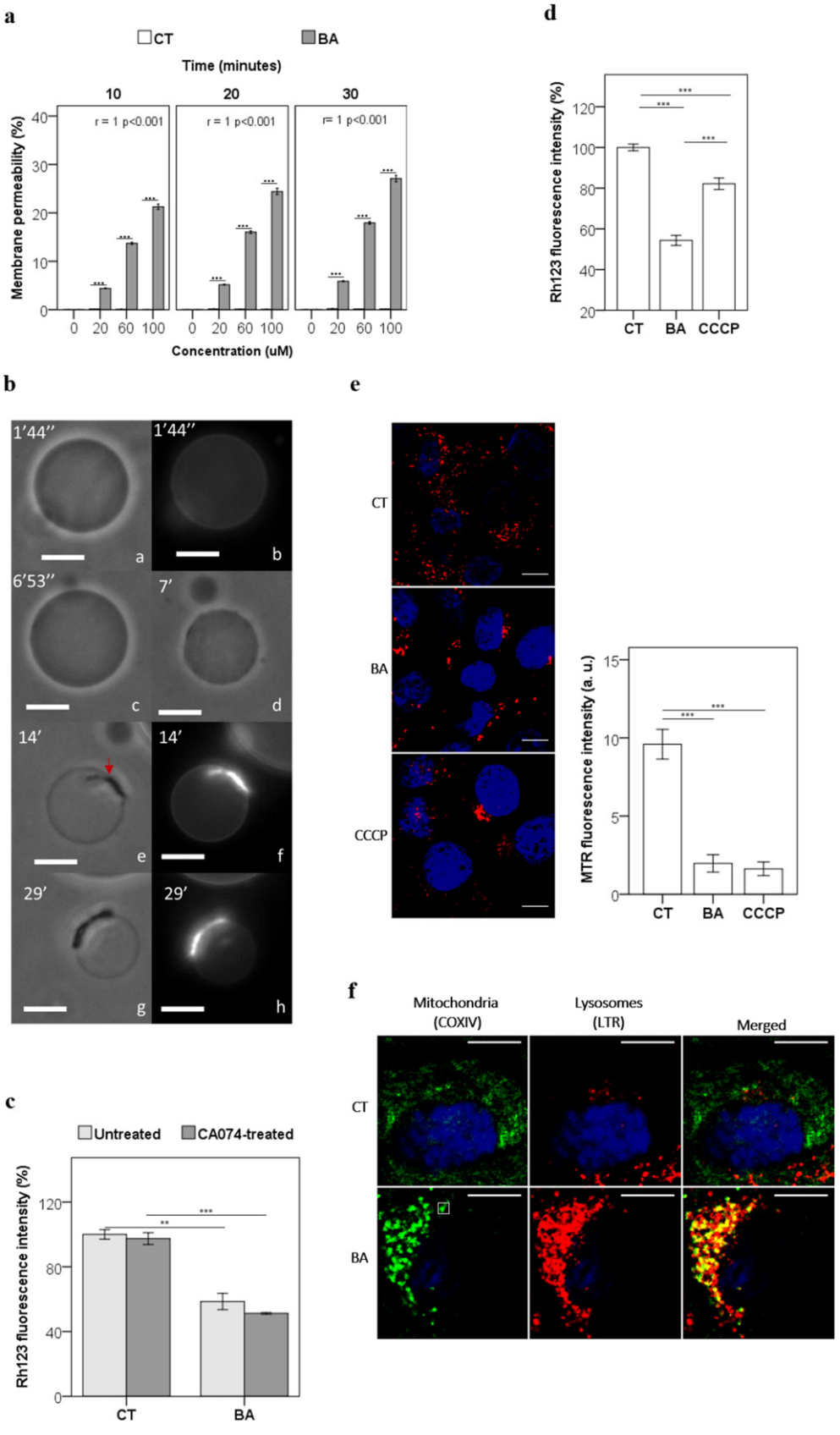

2.7. Liposome membrane permeabilization

To analyze the ability of BA to compromise membranes we used unilamellar liposomes as membrane-based model as described [21]. The membrane damage analysis is based on the release of carboxyfluorescein (CF, Sigma-Aldrich) from liposomes. The CF fluorescence at 517 nm was monitored as function of irradiation time at a controlled temperature with an Infinite M-200 Tecan microplate reader (Männedorf, Switzerland), operating with excitation at 480 nm. We calculated the rates of CF leakage as the percentage of total trapped CF release (Ft) under 0.2% (*v*/v) Triton X-100.

2.8. Live cell imaging and confocal microscopy

The lysosomotropic dye LysoTracker® Red DND-99 (LTR, Molecular Probes) was used as probe to stain acidic vacuoles [22], the MitoTracker® Green FM (MTG, Molecular Probes) to measure cellular mitochondria content, MitoTracker® Red CMH_2XRos (Molecular Probes) to monitor mitochondrial ROS and Hoechst® (Molecular Probes) to stain nuclei of live cells. In brief, to evaluate the double-staining of mitochondria and lysosomes after a 24 h-treatment with BA (20 μM), we incubated cells with LTR (200 nM), MTG (200 nM) and Hoechst® (5 μg/mL) in DMEM 1% (*v*/v) FBS for 15 min a 37 °C incubator at a moist atmosphere of 5% carbon dioxide. After chasing BA-challenged cells for 96 h (T4), we incubated HaCaT with MitoTracker® Red CMH_2XRos (1 μM) and Hoechst® (5 μg/mL) in DMEM 1% (*v*/v) FBS for 30 min a 37 °C incubator at a moist atmosphere of 5% carbon dioxide. Following washing, we immediately analyzed the Hoechst -counterstained slides under confocal microscope (Zeiss™ Axiovert 200 LSM 510 Laser and Confocor Modules) equipped with a Plan-APOCHROMAT 63×/1.40 oil DIC M27 objective (Zeiss™) and imaged using Image J Software (National Institutes of Health). We used filter sets that provide an excitation of 350, 488, 547 and 633 nm with emission band pass filters of 360–400 nm, 515–534 nm, 554–608 nm and 651–694 nm to detect the fluorescence of Hoechst®, MitoTracker® Green FM, LysoTracker® Red DND-99 and MitoTracker® Red CMXRos, respectively.

2.9. Immunocytochemistry and confocal microscopy

After a 24 h-treatment with BA (20 μM) the cells were washed and refreshed with DMEM (Sigma-Aldrich) supplemented with 10% (*v*/v) FBS, 100 U/mL of penicillin, and 100 pg/mL of streptomycin. After a period of 96 h (T4) the biological effects were evaluated. Following incubation with MTR (1 μM) for 30 min a 37 °C incubator at a moist atmosphere of 5% carbon dioxide, we performed fixation with cooled 4% (*w*/v) formaldehyde pH 7.2 in PBS. After washing and blocking, we incubated slides with primary mouse monoclonal antibody IgG2a against the cytochrome *c* oxidase subunit IV (COXIV, Molecular Probes, #A221347) according to manufacturer's instructions, and then with goat Alexa 488-coupled antibodies against mouse IgG (Molecular Probes). Alternatively, for immunostaining autophagic vacuoles after a 24 h-treatment with BA we incubated slides with primary rabbit monoclonal antibody IgG (D10E10, Cell signaling Technology®, #7695) against the ubiquitin binding protein sequestosome 1 (SQSTM1, p62) that plays an importante role as autophagic adaptor by binding to autophagosomal membrane protein LC3-II, and then with goat Alexa 546-coupled antibodies against rabbit IgG (Molecular Probes). At the same condition, following incubation with LTR as described above, we performed immunoassay for COXIV stained with goat Alexa 633-coupled antibodies against mouse IgG (Molecular Probes). After a 6 h-treatment with BA, lysosome membrane permeabilization was evaluated following incubation with LTR (200 nM) for 30 min a 37 °C incubator at a moist atmosphere of 5% carbon dioxide. After washing and fixation, slides were incubated with primary mouse monoclonal antibody IgG2a against cathepsin B (CTSB, Abcam®, # ab58802) and then with goat Alexa 488-coupled antibodies against mouse IgG (Molecular Probes). We analyzed the DAPI-counterstained slides as above by using filter sets that provide an excitation of 350, 488, 547 and 633 nm with emission band pass filters of 360–400 nm, 515–534 nm, 554–608 nm and 651–694 nm to detect the fluorescence of DAPI, Alexa-488, LysoTracker® Red DND-99 or Alexa-546 and MitoTracker® Red CMXRos or Alexa-633, respectively.

2.10. Assay for measuring of cathepsin B activity

After a 3 h-treatment with BA (20 μM), the activity of cytosolic cathepsin B (CTSB) was evaluated by using a fluorescence-based assay kit (BioVision Inc., # K140-100), which utilizes the preferred CTSB substrate sequence RR labeled with AFC (amino-4-trifluoromethyl coumarin). Briefly, treated-cells were lysed in 50 μL of chilled CB cell lysis buffer. After incubation on ice for 10 min and centrifugation at 10,000 *g* for 10 min at 4 °C, we obtained the cytosolic-fraction of CTSB that is capable of cleaving the synthetic substrate RR-AFC to release free AFC. After incubation protected from light at 37 °C for 1 h, the released AFC could easily be quantified using a fluorescence plate reader (SpectraMax® ie3 Microplate Detection Platform, Molecular Devices) with a 328 nm excitation filter and 460 nm emission filter. 15 μg of protein per sample was used for enzymatic assays whose concentration was measured using the BRADFORD assay (Quick Start™ Bradford Protein Assay, Bio—Rad Laboratories). Finally, the CTSB activity was normalized by total protein and expressed as arbitrary units (a. u.) after ratio to control (DMSO).

2.11. Mitochondrial function

After treatment with BA (20 μM), the following fluorescent probes were used to examine mitochondrial function, according to indicative times and manufacturer's instructions: 1) MitoTracker® Green FM (MTG, Molecular Probes) to measure cellular mitochondria content, and 2) Rhodamine 123 (Rh123, Sigma-Aldrich) and MitoTracker® Red CMH_2XRos (MTR, Molecular Probes) to monitor loss of mitochondrial membrane potential ($\Delta\Psi m$). Briefly, to monitor mitochondrial function we incubated cells with MTR (1 μM), MTG (200 nM) or Rh123 (500 nM) for 30 min in a 37 °C incubator at a moist atmosphere of 5% carbon dioxide. We used confocal microscopy to monitor mitochondrial function as described above. Alternatively, we measure mitochondrial dyes-related fluorescence (MTG) parallel to incorporation with Propidium iodide (PI, Sigma-Aldrich). Briefly, after BA-treatment at indicative time, HaCaT cells were washed and incubated with MTG

Fig. 2. BA damages membranes of mimetic systems and intracellular organelles. (a) Membrane permeability analysis according to CF-release from unilamellar liposomes after treatment with BA as a function of concentration (20–100 μM) and the time (10 to 30 min). Pearson's coefficient values in r. (b) POPC GUVs containing 0.2% (*w*/v) of Rhodamine-DPPE at different times after the initial contact with a solution containing BA (100 μM). Panels a, c, d, e and g are pictures obtained with the transmission mode and Panels b, f and h were obtained with the fluorescence mode. (c) FACS analysis of Rh123 loaded-mitochondria after treating HaCaT for 3 h with CT and BA in the presence (+) and absence (−) of 10 μM CA074, a specific inhibitor of CTSB. The mitochondrial membrane potential ($\Delta\Psi m$) was measured in terms of Rh123 cytofluorometry analysis and represented as percentage relative to control. (d) Following treatment of 3 h with CT, BA and 2 μM carbonyl cyanide m-chlorophenylhydrazone (CCCP), HaCaT was stained with Rh123 and analyzed by FACS. Bars represented the mean Rh123 fluorescence intensity calculated as percentage relative to control. (e) Micrographs of HaCaT treated with CT, BA and CCCP for 6 h and stained with MitoTracker® Red Red CMH_2XRos. At right, bars revealed the mean CMXRos red fluorescence intensity. (f) Right after a 24 h-treatment, CT and BA treated cells were stained with LysoTracker® Red DND-99 (LTR) and following immunostaining for the mitochondrial marker COXIV (green). The depicted mitochondrion is 2.1 μm long and 1.1 μm wide (square). Panels (a, c, d and e) showed mean ± standard error of three independent experiments are shown. The significance of differences after multiple or pair-wise comparisons was indicated as $^{*}P \le 0.01$; $^{**}P < 0.001$, $^{***}P < 0.0001$. Scales bar in (b), (e) and (f) are 10 μm.

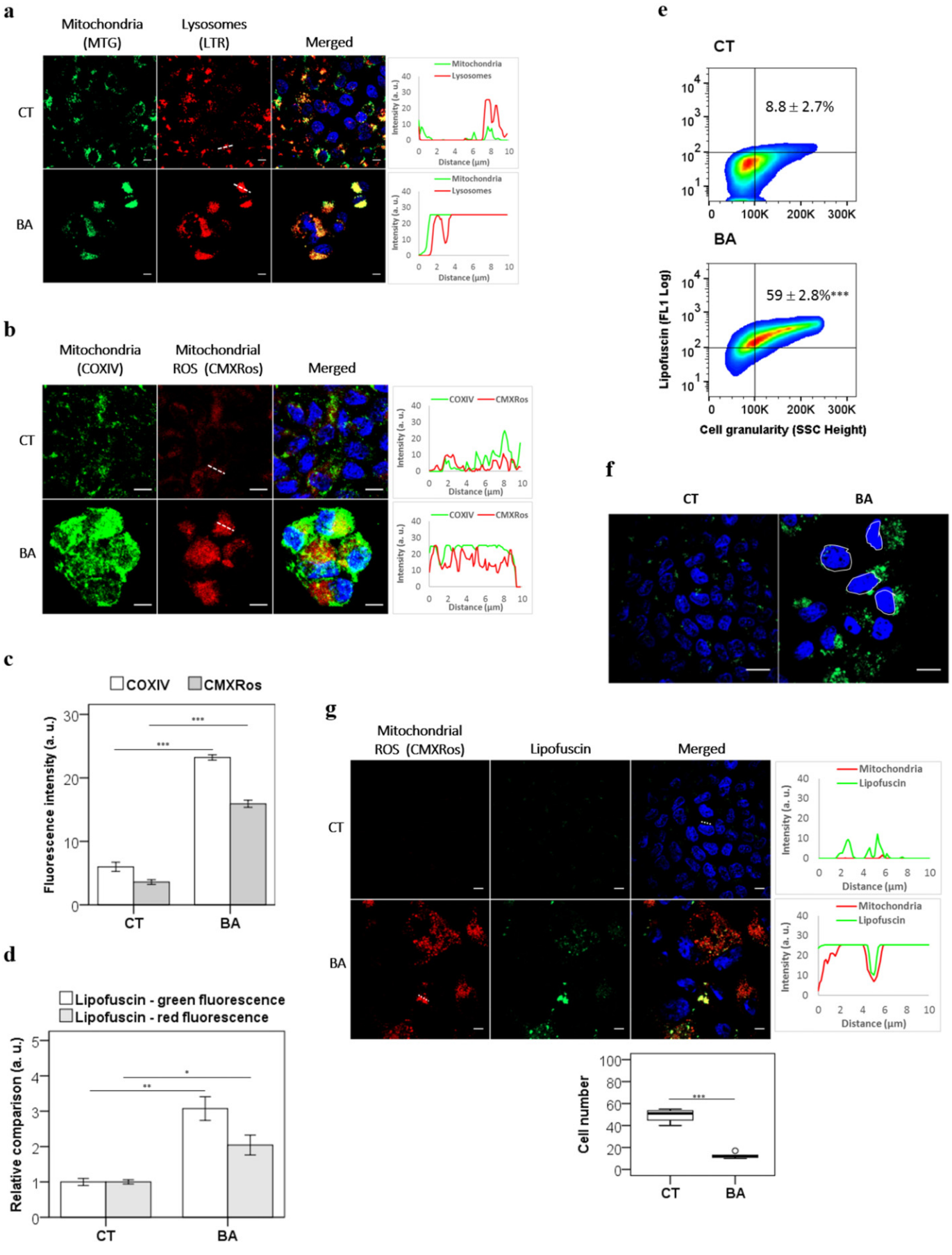
a
Mitochondria (MTG)
Lysosomes (LTR)
Merged
CT
BA
Mitochondria
Lysosomes
Intensity (a. u.)
Distance (μm)
b
Mitochondria (COXIV)
Mitochondrial ROS (CMXRos)
Merged
COXIV
CMXRos
c
Fluorescence intensity (a. u.)
d
Lipofuscin - green fluorescence
Lipofuscin - red fluorescence
Relative comparison (a. u.)
e
8.8 ± 2.7%
59 ± 2.8%***
Lipofuscin (FL1 Log)
Cell granularity (SSC Height)
f
g
Mitochondrial ROS (CMXRos)
Lipofuscin
Merged
Cell number

(200 nM) and PI (2 μg/mL) for 15 min in a 37 °C incubator at a moist atmosphere of 5% carbon dioxide. Next, MTG and PI fluorescences were detected by flow cytometry (BD FACSVerse™) using excitation laser at 488 nm (FL1) and 640 nm (FL3), respectively. At least 20,000 events were collected in each analysis and data was analyzed by FlowJo software.

2.12. Western blot

After a 6 h-treatment with BA (20 μM) and CQ (60 μM) cell lysates were prepared in lysis buffer - 20 mM Piperazine-*N*,*N*′-bis(2-ethanesulfonic acid) (PIPES, SigmaAldric), 100 mM NaCl (SigmaAldric), 1 mM EDTA (Ethylenediaminetetraacetic acid, Life Technologie®), 10% (*w*/*v*) sucrose (Sigma-Aldrich), 0.1% (*w*/*v*) 3-[(3-Cholamidopropyl)dimethylammonio]-1-propanesulfonate hydrate (CHAPS, Sigma-Aldrich), 0.1% (*v*/v) Triton X-100 (Sigma-Aldrich), 1 mM Phenylmethylsulfonyl fluoride (PMSF, Sigma-Aldrich), 5 μM Pepstatin A (Sigma-Aldrich), 50 μM digitonin (Sigma-Aldrich) and electrophoresis of total proteins (20 μg) was performed as previously described [16]. Briefly, after blockage in PBS with 5% (*v*/v) milk and 0.1% (*v*/v) Tween 20 (Sigma-Aldrich) for one hour at room temperature, membranes were incubated at 4 °C overnight with primary monoclonal anti-LC3-II (LC3B (D11) XP®, Cell Signaling Technology®, #3868) or for two hours at room temperature with anti-GAPDH (Sigma-Aldrich, # G9545). LC3B and GAPDH antibodies were diluted at 1:1000 and 1:10,000 in PBS with 2.5% (*v*/v) milk and 0.1% (*v*/v) Tween 20, respectively. After washing three times in PBS 0.1% (*v*/v) Tween 20 and incubation for 1 h at room temperature with secondary polyclonal antibody against Rabbit IgG (H + L) HRP-conjugated (KPL, # 074-1506) diluted in PBS with 2.5% (*v*/v) milk and 0.1% (*v*/v) Tween, membranes were washed twice in PBS 0.1% (*v*/v) Tween 20 and once in PBS, 10 min each. Next, membranes were incubated with Amersham® ECL Prime Western Blotting Detection Reagent (GE Healthcare Life Sciences) for five minutes, followed exposion to X-Ray films. Images (in TIFF files) were analyzed using Image J software and the results were normalized to GAPDH band intensities.

2.13. Detection of lipofuscin-like autofluorescence

One of the most important properties of lipofuscin is a broad spectrum of autofluorescence that can be detected by fluorescence/confocal microscopy or other methods such as flow cytometry, making possible its quantification [23]. Here, 96 h after BA treatment HaCaT cultured on coverslips were fixed with cooled 4% (*w*/*v*) formaldehyde pH 7.2 in PBS for 15 min, washed and were mounted in ProLong® gold antifade reagent containing DAPI nuclear stain (Molecular Probes). Autofluorescence of lipofuscin granules was then observed by excitation at 488 nm using a 501–520 nm band pass filter. Alternatively, 24 h after a 24 h-BA treatment (T2) cytofluorometric analysis (BD FACS Verse™) of live cells were performed to quantify lipofuscin autofluorescence regarding the FL1 (excitation with blue light at 488 nm) and FL3 (excitation with red light at 640 nm) parameters.

2.14. Senescence-associated β-galactosidase activity

The replicative senescence was evaluated by SA-βgal assay, as described before [24]. After a 24 h-treatment with BA (20 μM) the cells were washed and refreshed with DMEM (Sigma-Aldrich) supplemented with 10% (*v*/v) FBS, 100 U/mL of penicillin, and 100 pg/mL of streptomycin. At T4 cells were fixed with methanol and visualized using an inverted microscope for transmitted light (Zeiss™ Axiovert 200 LSM 510 Laser and Confocor Modules). The proportion of cells positive for SA-βgal activity was quantified according to plugin Segmentation analysis supplied by Image J Software.

2.15. Cell clonogenic assay

Clonogenic assay is based on the ability of a single cell to grow into a colony, defined here to consist of at least 40 cells. After treatment with BA (20 μM) for 24 h, HaCaT was seeded out in appropriate dilutions to form colonies in one week. Next, colonies were fixed with methanol and stained with Crystal Violet (CV) 0.02% (*w*/*v*) solution and counted. The fixed CV-stained colonies were visualized using an inverted microscope for transmitted light (Zeiss™ Axiovert 200, Germany) and imaged using Image J Software.

2.16. Genome instability analysis

At T4 G2/M cells were observed. Cell cycle distribution was examined with Propidium Iodide (PI, Sigma-Aldrich) staining. In brief, cells were harvested and fixed with 70% (*v*/v) ethanol for at least 24 h. After fixation, cells were washed twice with PBS, followed by incubation with PBS containing 20 μg/mL PI and 0.2 mg/mL RNase A (Invitrogen®) for 30 min at 37 °C. The fluorescence emission was analyzed by flow cytometry (BD FACSCalibur™), using excitation laser at 635 nm (FL3). At least 20,000 events were collected in each analysis. Data was further analyzed by FlowJo software, using the cell cycle tool.

2.17. Nuclear morphometric analysis

To perform Nuclear Morphometric Analysis (NMA) of treated cells (as described before) at T4 nuclei were stained with DAPI and pictures were taken on a fluorescent inverted microscope (Zeiss™ Axiovert 200 LSM 510 Laser and Confocor Modules). By using the Image J Software's NII Plugin we analyzed parameters of nuclear size and shape for a large population of cells [25]. These parameters were features regard with Aspect (Asp), Area box (Arbx), Radius ratio (Rr) and Roundness (Rou), and combined in an index called Nuclear Irregularity Index [NII = Asp − Arbx + Rr − Rou] [25].

2.18. Statistics

Statistical analysis was performed using IBM® SPSS Statistics version 20. To perform comparative statistical analysis, we first analyzed the normal distribution of data according to Kolmogorov-Smirnoff test. Next, we performed pair-wise comparisons for independent samples

Fig. 3. Autophagy impairment and lipofuscinogenesis. (a) Long after acute effects of BA (T4), HaCaT was stained with Hoechst® (nuclei), MitoTracker® Green FM (mitochondria) and LysoTracker® Red DND-99 (lysosomes). Line scans show the co-localization between mitochondria (green) and lysosome (red) and correlate to the lines drawn in the micrographs (right panel). (b) At T4 HaCaT was stained with MitoTracker® Red CMH_2XRos that once oxidized generate CMXRos, whose fluorescence intensity is proportional to mitochondrial ROS. Cells were then immunostaining with mitochondrial marker COXIV (mitochondrial mass). At right, line scans show the co-localization between mitochondria marker COXIV (green) and CMXRos (red) and correlate to the lines drawn in the images. (c) Bars showed mean fluorescence intensity for COXIV and CMXRos determined in (b). (d) At T2 FACS analysis of lipofuscin autofluorescence regarding the FL1 (excitation with blue light) and FL3 (excitation with red light) parameters. Red and green lipofuscin fluorescences were weighted by control and represented as arbitrary units (a. u.). (e) At same condition before, representative scatter-plots showing the significant higher frequency of lipofuscin-loading in vacuolated cells (SSC^+). (f) At T4 larger cells showed significant increase in lipofuscin-loading and nuclear augmentation (depicted area) after BA as revealed by confocal microscopy. (g) Following the same condition above, micrographs of treated HaCaT showed mitochondrial oxidation of MitoTracker® Red CMH_2XRos that leads to red fluorescent CMXRos. Images were obtained to show either CMXRos fluorescence (excitation at 547 nm/emission 554–608 nm) or lipofuscin particles fluorescence (excitation at 488 nm/emission 501–520 nm). Line scans show the co-localization between lipofuscin (green) and CMXRos (red) and correlate to the lines drawn in the images (right panel). In order to quantify the red fluorescence due to the presence of CMXRos at similar contrast ratio to that of lipofuscin, we set the microscopy gain to a minimum threshold, and applied it to control and to BA-treated cells. Bars represented count cell number of several micrographs at T4. Mean ± standard error of three independent experiments are shown. The significance of differences after BA in comparison to control (CT) was indicated $^*P < 0.05$; $^{**}P < 0.01$; $^{***}P < 0.0001$. Scales bar in (a), (b), (f) and (g) are 10 μm.

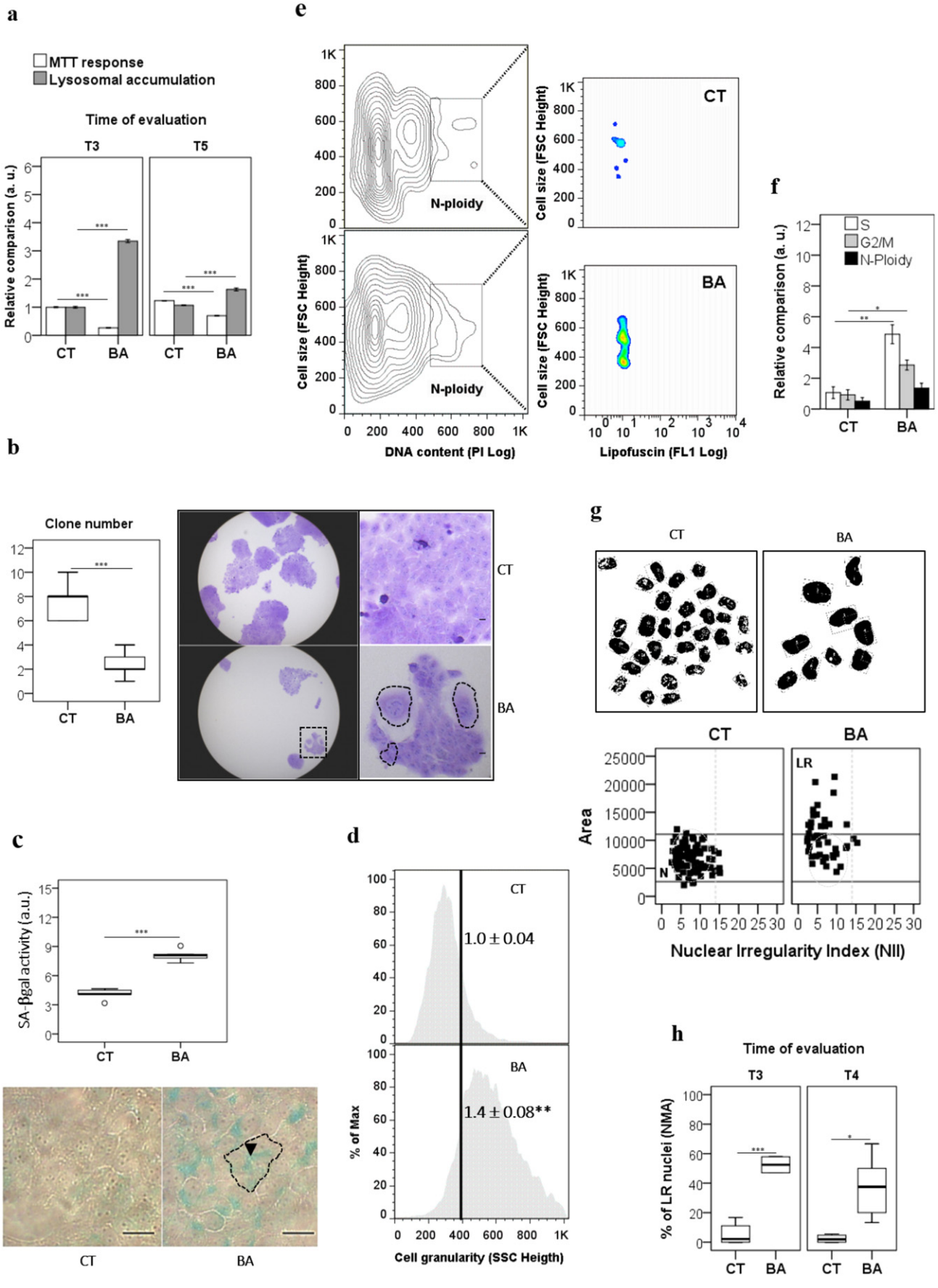
a
MTT response
Lysosomal accumulation
Time of evaluation
T3
T5
Relative comparison (a. u.)
CT
BA
CT
BA
e
N-ploidy
N-ploidy
Cell size (FSC Height)
DNA content (PI Log)
CT
BA
Lipofuscin (FL1 Log)
f
S
G2/M
N-Ploidy
Relative comparison (a. u.)
CT
BA
b
Clone number
CT
BA
CT
BA
g
CT
BA
CT
BA
LR
N
Area
Nuclear Irregularity Index (NII)
c
SA-βgal activity (a.u.)
CT
BA
CT
BA
d
CT
1.0 ± 0.04
BA
1.4 ± 0.08**
% of Max
Cell granularity (SSC Heigth)
h
Time of evaluation
T3
T4
% of LR nuclei (NMA)
CT
BA
CT
BA

using the parametric or non-parametric tests T-student or Mann-Whitney, respectively. In case of multiple comparisons, we performed one-way analysis of variance (ANOVA) with Dunnett's T3 or Bonferroni post-hoc tests, depending on homogeneity of variance. The strength of linear correlation analysis was calculated by Pearson's coefficient (r). We analyzed data obtained from at least three independent experiments, expressed as mean values ± standard error. We considered *P*-values lower than 0.05 statistically significant. The significance of differences was depicted with asterisks.

3. Results

Two experimental systems were employed in this work: HaCaT cells in culture and membrane mimetic systems. Periods of incubation of BA with membrane mimics varied and are reported in each individual experiment. In the case of cells, all experiments were performed after a 24 h incubation with 20 μM Betulinic Acid (BA) and 0.25% (*v*/v) DMSO (CT). Cells were refreshed with medium and studied right after BA incubation (T1) and in sequential periods of: 24 h (T2), 48 h (T3) or 96 h (T4).

3.1. BA causes cell death and/or growth arrest associated with autophagy inhibition and accumulation of mitochondria

Right after treating HaCaT cells with BA (T1), microscopic analysis showed noteworthy accumulation of AO-stained acidic vacuoles and enlarged dead cells (Fig. 1a). Cytometry analysis confirmed the prevalence of enlarged-vacuolated cells compared to control, which were also significantly enhanced at T2 (Fig. 1b). Cells that were kept alive after BA showed extensive vacuolization and nuclei enlargement (Fig. 1c). The accumulation of acidic vacuoles was linearly correlated to a smaller MTT response compared to control. Note that this correlation was strong over the time (Table 1).

The lack of increase in MTT over time suggests that the cellular viability is not reestablished after BA (Table 1). In order to evaluate the proliferative rate of HaCaT cells after BA we also analyzed CVS labelling (Fig. 1d). Control cells showed a significant increase in cell growth strongly correlated with time, unlike BA-treated cells that showed almost no increase in CVS.

The accumulation of acidic vacuoles indicates that BA may decrease cell growth due to the catabolic malfunction of autophagy [26]. Indeed, right after BA we observed a huge accumulation of autophagy substrates (p62 and LC3-II) even in the absence of the inhibitor of autophagic flux Bafilomycin *A*1 (BAF-*A*1). Of note, in control cells increased levels of p62 and LC3-II were only observed in the presence of BAF-*A*1 (Supplementary Fig. 1a).

Under an interruption of autophagic flux induced by BAF-*A*1, it is also possible to correlate autophagosome (AP) synthesis with changes in LC3-II levels [22]. We also used Chloroquine (CQ) as a positive control of autophagy inhibition [15,27]. Both BA and CQ significantly increased LC3-II levels even in the absence of BAF-*A*1 (Supplementary Fig. 1b). CQ associated with BAF-*A*1 significantly increased LC3-II levels compared to BAF-*A*1 only, indicating higher AP synthesis [28]. On the other hand, in BA-treated cells there was no further increase in LC3-II upon BAF-*A*1 treatment, indicating a blockage in LC3-II degradation (Supplementary Fig. 1b). Indeed, BA does not affect AP transport to lysosomes, but hampers degradation of damaged mitochondria within impaired lysosomes [16]. To investigate whether undigested mitochondria accumulated after BA, vacuolated cells were gated (see Fig. 1b) in terms of plasma membrane permeabilization (PI^+), a common hallmark of cell death, and mitochondria mass (MTG^+) (Supplementary Fig. 1c). Right after BA treatment (T1), we observed a remarkable mitochondria accumulation in a subset of dead cells (58%). This observation was also significant at T2 on a subset of 29% dead cells (Supplementary Fig. 1c). It is clear, therefore, that BA compromises autophagic flux resulting in a huge accumulation of undigested mitochondria and autophagy-associated cell death [16].

3.2. The effect of BA in membrane mimics illustrates the damage in membranes of cell organelles

Several reports showed that BA induces cell death through a not completely understood mitochondria-dependent mechanism [16,17,29]. BA interacts with pure phospholipid membranes, being capable of changing their permeability [16,30,31]. In order to provide further insights into the ability of BA to disrupt membranes, we characterized its interaction with more simplistic membrane mimetic systems, i.e., liposomes and giant unilamellar vesicles (GUVs). BA increased the permeability of carboxyfluorescein (CF) in liposomes as a function of concentration and time, showing elevated Pearson's linear coefficient in comparison with control liposomes that had no leakage (Fig. 2a). Within 10 min of BA addition there was a 4.8 fold increase in membrane leakage as a function of concentration (20 versus 100 μM). The increase in CF release at a given concentration (for example 100 μM) was also substantial in regard with time. There is a 1.3 fold increase comparing 10 versus 30 min (Fig. 2a).

To analyze the physical damage in membranes we evaluated under an optical microscope the kinetics of the loss of membrane integrity of GUVs dispersed in a solution containing BA (100 μM). Phase contrast and fluorescence images were captured at different times after BA incubation. Representative images of events common to all ~100 vesicles observed in three independent experiments are shown in panels *a*, *c*, *d*, *e* and *g* of Fig.2b. Approximately 7 min after the initial contact with BA, GUVs shrank significantly and emitted membrane buds (panel *d*). Such events are followed by contrast loss as visualized on panels *e* and *g*. Remarkably, there is a filament-like accumulation of lipids in part of the membrane surface (red arrow, panel *e*) as observed both in phase contrast (panels *e* and *g*) and fluorescence modes (panels *f* and *h*). As described in liposomes (Fig. 2a), GUVs also showed an increase in membrane permeability that can be clearly perceived by the loss of the optical contrast across the membrane (Fig. 2b, panels *c* to *e*).

We asked if these events would lead to damage in intracellular organelles such as lysosome and mitochondria. Accordingly, we detected a significant increase in lysosomal membrane permeabilization in HaCaT, as measured by the increase in cytosolic cathepsin B (CTSB) activity (Supplementary Fig. 1d). The loss of lysosomal membrane integrity with subsequent cytosolic immunostaining of total CTSB in BA-treated cells also supported this finding (Supplementary Fig. 1e). We

Fig. 4. BA induces genomic instability and replicative senescence. 48 h (T3), 96 h (T4) or 120 h (T5) after a 24 h-treatment with 20 μM Betulinic Acid (BA) and 0.25% (*v*/v) DMSO (CT), HaCaT response was evaluated as described below. (a) At T3 and T5 after acute effects of BA, both MTT reduction and lysosome accumulation were determined and rated according to the treatment with CT detected at T3. (b) At T4 number of colonies of treated cells represented in box-plots. Micrographs showing cytochemical staining with CV of senescent cells after BA at T4. (c) At T4 cytochemical quantification of SA-β galactosidase activity after BA. Micrographs showed significant increase in activity of SA-β galactosidase in BA compared to CT. Bars represented count colony number of several micrographs. (d) At T4 following FACS cell analysis. Granularity (SSC Height) of HaCaT was represented by density histograms showing percentage of maximum values after BA. (e) At T4 following DNA staining with PI treated cells were analyzed by FACS. Scatter-plots contour log showing correlated two-parameters - DNA content (PI excited with red light, FL3) and cell size (FSC Height). At right, scatter-plots showing correlated two-parameter – lipofuscin (emission after blue light excitation, FL1) and cell size (FSC Height) in those cells with N-ploidy (squares). (f) According to cell cycle Watson distribution (FlowJo Software), box-plots showed arbitrary values of G2, S and N-ploidy (Super G2) relative to CT. (g) At T4 micrographs of HaCaT regard with the Nuclear Morphometric Analysis (NMA). Scatter-plots showing the population distribution of treated-cells according to nuclear area and Nuclear Irregularity Index (NII). (h) Bars showed the percentage of LR nuclei identified after NMA. Mean ± standard error of three independent experiments are shown. The significance of differences after BA in comparison to control (CT) was indicated $^*P < 0.01$; $^{**}P < 0.001$, $^{***}P < 0.0001$. Scales bar in (b) and (c) are 20 μm.

also observed a significant loss of mitochondrial membrane potential (ΔΨm) after BA (Fig. 2c). It is important to emphasize that released CTSB was not responsible for the damage in the mitochondrial membrane (Fig. 2c). Upon inhibition of CTSB activity by its specific inhibitor CA074, BA still induced a significant loss of ΔΨm, indicating that the impairment in mitochondria membrane was directly caused by BA. It is noteworthy that the loss of ΔΨm after BA was at least 2.5-fold more severe than that induced by the mitochondrial uncoupling agent carbonyl cyanide m-chlorophenylhydrazone (CCCP) [32] (Fig. 2d). Interestingly, only at longer exposition periods the loss of ΔΨm in CCCP-treated cells reached the intensity observed for BA (Fig. 2e). Therefore, it is clear that the disruption of the mitochondrial membrane integrity was faster after BA than CCCP, in accordance with the high efficiency of BA to interact and disturb membranes.

Likewise, right after BA treatment HaCaT showed a significant change in mitochondrial morphology resulting in enlarged mitochondrion with 2.1 μm long and 1.1 μm wide (Fig. 2f). Note that mitochondria engulfment by autophagic vacuoles was expressive in BA-treated cells. Under such toxic effects on mitochondria, HaCaT activates mitophagy [16]. However, BA also damages lysosomes and impairs autophagy that fails to rescue cells, which in turn leads to other outcomes, including decreased proliferation and cell death with inhibited autophagy (Fig. 1). We continue this investigation by characterizing the consequences of continuous accumulation of enlarged acidic vacuoles [16] and the subsequent induction of abnormal nuclei enlargement (Fig. 1c) in BA-treated cells.

3.3. BA induces genomic instability and replicative senescence

Several reports indicate that modulators of autophagy can promote cellular senescence in cultured cells as reviewed recently [22]. One of the possible outcomes of impaired autophagy is the accumulation of damaged mitochondria and lipofuscin [33,34]. We found that mitochondria accumulates within BA-damaged lysosomes [16] (Fig. 3a), especially in regions with extensive redox misbalance (elevated CMXRos fluorescence) (Fig. 3b and c), which are conditions that could favor lipofuscinogenesis [26,35]. Indeed, BA-treated cells showed significant increase in green (3.5 fold) and red (2.0 fold) autofluorescence of lipofuscin compared to control (Fig. 3d). The prevalence of lipofuscin-loaded cells was significantly higher after BA, with a 5-fold increase in vacuolated cells (Fig. 3e). Being rich in redox-active iron, lipofuscin itself continuously sustains oxidative stress [36] hampering lysosomal activity, thus aggravating damage on this organelle in long-term response [37]. In fact, at T4 lipofuscin accumulation was associated with increase in cell and nuclei size (Fig. 3f), and in mitochondrial oxidative stress and nuclear abnormalities (Fig. 3g). Thus, BA treatment compromises genomic stability by initially damaging lysosomal and mitochondrial membranes.

To further evaluate senescence in BA-treated cells, we analyzed their proliferation status. Over time, we noted a significant decrease in MTT response parallel to a lysosomal accumulation only in BA-treated cells (Fig. 4a). The significant decrease in the proliferation of cells after BA was confirmed by clonogenic assay (Fig. 4b). In fact, BA-treated cells showed hypertrophy with multiple or enlarged nuclei as depicted by traced-line (Fig. 4b), a typical aged-phenotype suggestive of cellular senescence [38].

In an attempt to further investigate the ability of BA to induce senescence, we evaluated common senescence markers: lack of cell proliferation, cell morphology (large and flat cells), senescence-associated beta-galactosidase (SA-βgal), aneuploidy and tetraploidy in G2/M cells, as reviewed [39]. As observed in the micrograph a significantly higher proportion of SA-βgal positive cells were observed after BA (Fig. 4c), and the typical senescence phenotype, which consisted of vacuolated cells with enlarged nuclei (traced line), was visible in BA-treated cells (black arrow).

The shift in the cell-cycle phases is another strong indication that BA favors arrest of cell growth [40,41]. At T4, cells showed an increase in cell granularity and heterogeneity of up to 1.4 fold (Fig. 4d). In addition, in BA-induced senescent cells we observed a significant arrest in S and G2 phases of cell cycle given by Watson distribution (Fig. 4e). Note that among BA-treated cells there was a sizable fraction of cells with 4 N DNA content, and some with chromosomal aberrations including polyploidy (square, Fig. 4e). Interestingly, polyploid cells also contained lipofuscin (Fig. 4e). Note also that all three parameters of growth arrest were altered in BA-treated cells, including N-ploidy cells (Fig. 4f). Therefore, BA-treated cells developed characteristic morphological changes associated with senescence, including enlarged and often irregular nuclei and chromatin reorganization, in which the loss of nuclear stability and chromatin structure is highlighted [1,25,40].

To address the BA effects on nuclear morphology related to senescence in a long-term response we used the Image Plugin Nuclear Morphometric Analysis (NMA). This tool allowed us to quantify nuclear abnormalities specifically by calculating the Nuclear Irregularity Index (NII) [25]. We observed at T4 in BA-treated cells morphological appearances of LR (large and regular) nuclei, which are suggestive of senescence (Fig. 4g). Note that in BA-treated cells, several nuclei showed an area above the "normal ellipse N" (upper left quadrant, Fig. 4g). The frequency of LR-nuclei did not change as a function of time (Fig. 4h). Even at T3, we noted a significant increase in the frequency of BA-treated cells with senescent nuclei having morphometric LR-alteration that remained significantly elevated at T4 (Fig. 4h). These morphological characteristics of the nuclei are another indication that BA triggers cellular senescence. Lipofuscinogenesis-induced increment in N-ploidy cells closed the link between disorganization of lipid bilayers and the consecutives cell responses: mitophagy impairment, genomic instability and cellular senescence, as summarized in Fig. 5.

4. Discussion

Cellular senescence is a generic response of persistent growth arrest as a consequence of sub-lethal stresses in both normal non-transformed and immortalized transformed cells [2]. The relationship between senescence induction and the status of autophagy is still controversial since senescent phenotypes have been related to both activation or inhibition of autophagy, depending on the mechanism of senescence induction [8,9,42].

The damage in lysosomal function caused by BA cannot be explained by traditional mechanisms, including lack lysosome acidification or neutralization of its internal pH. Otherwise, BA disturbs lysosome's membrane integrity what dramatically jeopardizes lysosomal function, leading to a lysosomal-mitochondrial axis of cellular stress that causes autophagy-associated cell death [16]. Moreover, in surviving BA-challenged cells there is sustained formation of reactive oxygen species inside non-functional lysosomes, which in a long-term response leads to lipofuscinogenesis, genomic instability and cell senescence (Fig. 5). Therefore, in cells with higher intracellular BA concentration, there is a larger accumulation of non-functional lysosomes intrinsically related to autophagy-associated cell death, as summarized in Fig. 5. On the other hand, in a set of HaCaT in which BA uptake was smaller there is also damage in lysosomes and mitochondria sustaining an imbalance in the cellular redox. However, this imbalance is not enough to induce cell death, but will culminate in aging and senescence [11]. We are planning a new study aiming to determine the BA concentration threshold that will cause a shift from senescence to death. However, it is clear that promotion of concomitant damage in mitochondrial and lysosomal membranes seems to be an efficient strategy for inducing both autophagy-associated cell death and cell aging.

Agents that generate oxidative stress, DNA damage and/or stress-related signaling induce cellular senescence [2]. Our data showed that BA triggers premature senescence in keratinocytes by destabilizing lipid bilayers, damaging lysosome and mitochondria membranes,

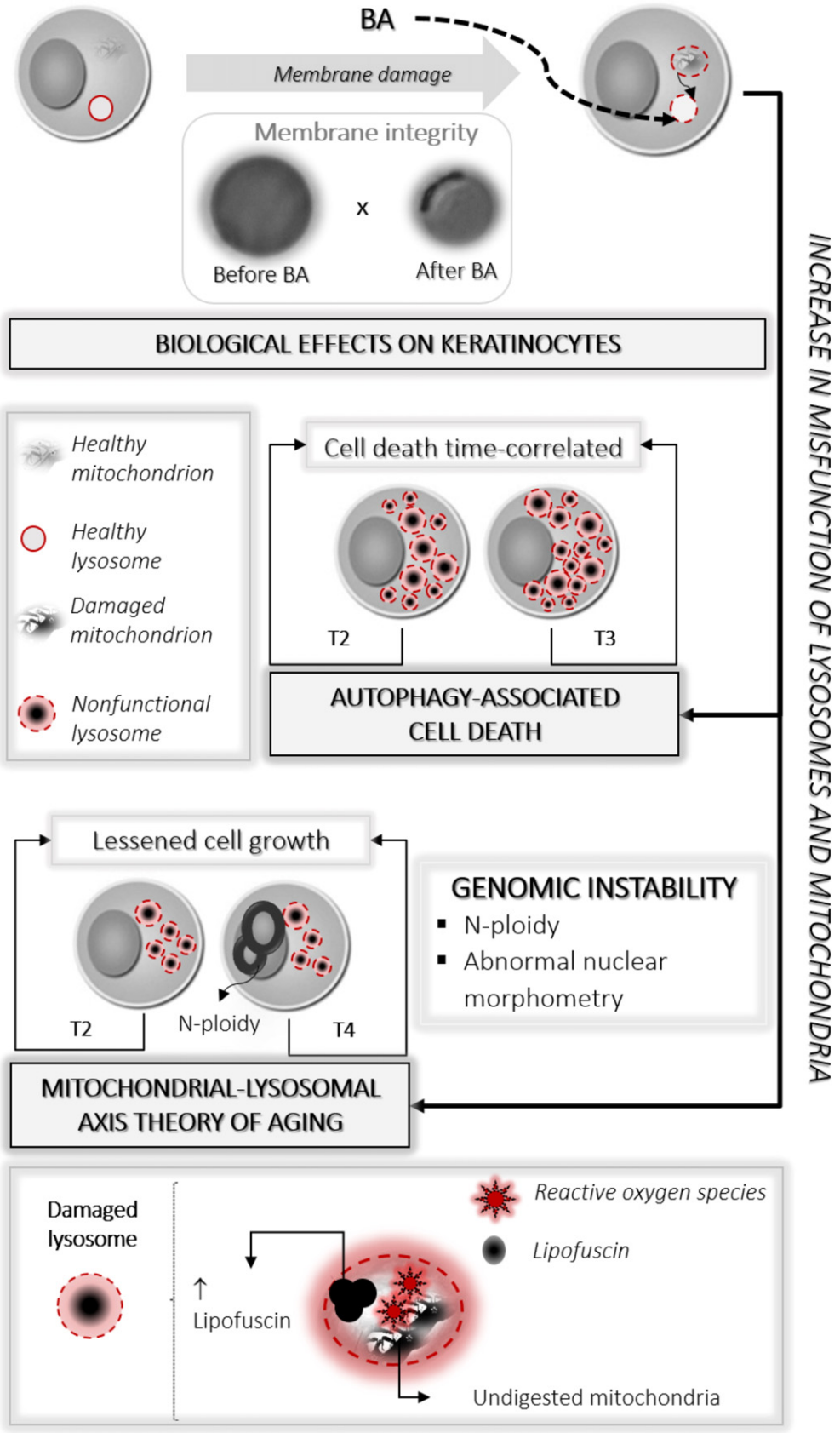

Fig. 5. Main hypothesis proposed: Mitochondrial-lysosomal axis theory of aging associated with membrane damage by BA causing lipofuscinogenesis and cell senescence in HaCaT human keratinocytes. This figure was drawn by W. K. M.

which leads to genomic instability and cell senescence. This work contributes to the theory of Brunk and Terman [8], defining a clear trigger to the imbalance in the mitochondrial-lysosomal axis. Also, the finding that the initial molecular trigger of BA-induced senescence is the disorganization of membrane lipids indicates that genomic instability can also be indirectly caused by lipid disorganization, and not only by defects in the DNA repair pathways [43].

Many BA derivatives have been synthesized to improve the weak solubility of parent BA and to increase its selectivity toward tumor cells [44]. It will be quite interesting to study the effect of BA derivatives on model membranes. We believe that the association with selective disorganization of organelles' membranes represents a promisor strategy to uncover the anti-tumor activities of novel lead compounds. In fact, cellular senescence must be one of the main mechanisms of action of BA derivatives.

5. Conclusions

BA destabilizes lipid bilayers, damaging mitochondria and lysosome membranes and causing autophagy impairment. This scenario increases levels of aged mitochondria, lipofuscin and genomic instability (N-ploidy cells), culminating in cell senescence. In this work, we were able to correlate cell senescence with a direct physical damage in the membranes of two key intracellular organelles, i.e., mitochondria and lysosome, and to link the biological effects of BA with senescence. We are confident that using BA as experimental model in different cell types will allow a better understanding of the mechanistic link between compromised mitophagic flux and genomic instability.

Supplementary data to this article can be found online at http://dx.doi.org/10.1016/j.bbagen.2016.10.018.

Author contributions

W.K.M. and M.S·B. designed research; W.K.M. conceived and designed the experiments; W.K.M, A.B.G. and H.J. performed research; E.T.C., B.S.S. and R.I. contributed new reagents/analytic tools; W.K.M., A.B.G., E.T.C., B.S.S., R.I. and M.S.B analyzed data; and W.K.M. and M.S.B. wrote the main manuscript text, and all authors reviewed the manuscript.

Additional information

The authors declare no competing financial interests.

Transparency Document

The Transparency document associated with this article can be found, in the online version.

Acknowledgements

The authors are grateful to Alessandra A. A. de Sousa, Cleidiane Souza, Ana C. Viotto and Edson Alves for technical assistance; Adriana Y. Matsukuma and Wilton J. *R. Lima* for helping in confocal microscopy and flow cytometry. This work was supported by Programa Nacional de Pós Doutorado (PNPD)/Coordenação de Aperfeiçoamento de Pessoal de Nível Superior (CAPES)/Financiadora de Estudos e Projetos (FINEP), Brazil [grant number 02533/09-0] and by Fundação de Amparo à Pesquisa do Estado de São Paulo (FAPESP), Brazil [grant numbers 2012/50680-5, 2013/07937-8]. M.S.B. and R.I. are sponsored by Research fellowships from Conselho Nacional de Desenvolvimento Científico e Technológico (CNPq).

References

[1] C. López-Otín, M.A. Blasco, L. Partridge, M. Serrano, G. Kroemer, The hallmarks of aging, Cell 153 (2013) 1194–1217, http://dx.doi.org/10.1016/j.cell.2013.05.039.
[2] J.A. Ewald, N. Peters, J.A. Desotelle, F.M. Hoffmann, D.F. Jarrard, A high-throughput method to identify novel senescence-inducing compounds, J. Biomol. Screen. 14 (2009) 853–858, http://dx.doi.org/10.1177/1087057109340314.
[3] L. Hayflick, P.S. Moorhead, The serial cultivation of human diploid cell strains, Exp. Cell Res. 25 (1961) 585–621, http://dx.doi.org/10.1016/0014-4827(61)90192-6.
[4] T. von Zglinicki, R. Pilger, N. Sitte, Accumulation of single-strand breaks is the major cause of telomere shortening in human fibroblasts, Free Radic. Biol. Med. 28 (2000) 64–74.
[5] M. Collado, M. Serrano, The power and the promise of oncogene-induced senescence markers, Nat. Rev. Cancer 6 (2006) 472–476, http://dx.doi.org/10.1038/nrc1884.
[6] T. Kuilman, C. Michaloglou, W.J. Mooi, D.S. Peeper, The essence of senescence, Genes Dev. 24 (2010) 2463–2479, http://dx.doi.org/10.1101/gad.1971610.
[7] D.C. Rubinsztein, G. Mariño, G. Kroemer, Autophagy and aging, Cell 146 (2011) 682–695, http://dx.doi.org/10.1016/j.cell.2011.07.030.
[8] U.T. Brunk, A. Terman, The mitochondrial-lysosomal axis theory of aging, Eur. J. Biochem. 269 (2002) 1996–2002, http://dx.doi.org/10.1046/j.1432-1033.2002.02869.x.
[9] A. Terman, T. Kurz, M. Navratil, E.A. Arriaga, U.T. Brunk, Mitochondrial turnover and aging of long-lived postmitotic cells: the mitochondrial-lysosomal axis theory of aging, Antioxid. Redox Signal. 12 (2010) 503–535, http://dx.doi.org/10.1089/ars.2009.2598.
[10] T. Kurz, A. Terman, U.T. Brunk, Autophagy, ageing and apoptosis: the role of oxidative stress and lysosomal iron, Arch. Biochem. Biophys. 462 (2007) 220–230, http://dx.doi.org/10.1016/j.abb.2007.01.013.
[11] A. Terman, Catabolic Insufficiency and Aging, Ann. N. Y. Acad. Sci., 2006, pp. 27–36, http://dx.doi.org/10.1196/annals.1354.005.
[12] E. Aymard, V. Barruche, T. Naves, S. Bordes, B. Closs, M. Verdier, M.-H.H. Ratinaud, Autophagy in human keratinocytes: an early step of the differentiation? Exp. Dermatol. 20 (2011) 263–268, http://dx.doi.org/10.1111/j.1600-0625.2010.01157.x.
[13] S. Fulda, G. Kroemer, Targeting mitochondrial apoptosis by betulinic acid in human cancers, Drug Discov. Today 14 (2009) 885–890, http://dx.doi.org/10.1016/j.drudis.2009.05.015.
[14] L. Yang, Y. Chen, J. He, S. Yi, L. Wen, J. Zhao, B. Zhang, G. Cui, Betulinic acid inhibits autophagic flux and induces apoptosis in human multiple myeloma cells in vitro, Acta Pharmacol. Sin. 33 (2012) 1542–1548, http://dx.doi.org/10.1038/aps.2012.102.
[15] W.K. Martins, D. Severino, C. Souza, B.S. Stolf, M.S. Baptista, Rapid screening of potential autophagic inductor agents using mammalian cell lines, Biotechnol. J. 8 (2013) 730–737, http://dx.doi.org/10.1002/biot.201200306.
[16] W.K. Martins, É.T. Costa, M.C. Cruz, B.S. Stolf, R. Miotto, R.M. Cordeiro, M.S. Baptista, Parallel damage in mitochondrial and lysosomal compartments promotes efficient cell death with autophagy: the case of the pentacyclic triterpenoids, Sci. Rep. 5 (2015) 12425, http://dx.doi.org/10.1038/srep12425.
[17] L. Potze, F.B. Mullauer, S. Colak, J.H. Kessler, J.P. Medema, Betulinic acid-induced mitochondria-dependent cell death is counterbalanced by an autophagic salvage response, Cell Death Dis. 5 (2014), e1169 http://dx.doi.org/10.1038/cddis.2014.139.
[18] D.V. Raghuvar Gopal, A.a. Narkar, Y. Badrinath, K.P. Mishra, D.S. Joshi, Betulinic acid induces apoptosis in human chronic myelogenous leukemia (CML) cell line K-562 without altering the levels of Bcr-Abl, Toxicol. Lett. 155 (2005) 343–351, http://dx.doi.org/10.1016/j.toxlet.2004.06.015.
[19] P. Boukamp, R.T. Petrussevska, D. Breitkreutz, J. Hornung, A. Markham, N.E. Fusenig, Normal keratinization in a spontaneously immortalized aneuploid human keratinocyte cell line, J. Cell Biol. 106 (1988) 761–771.
[20] O. Mertins, I.O.L. Bacellar, F. Thalmann, C.M. Marques, M.S. Baptista, R. Itri, Physical damage on giant vesicles membrane as a result of methylene blue photoirradiation, Biophys. J. 106 (2014) 162–171, http://dx.doi.org/10.1016/j.bpj.2013.11.4457.
[21] D. Rodrigues, A.C. Viotto, R. Checchia, A. Gomide, D. Severino, R. Itri, M.S. Baptista, W.K. Martins, Mechanism of *Aloe Vera* extract protection against UVA: shelter of lysosomal membrane avoids photodamage, Photochem. Photobiol. Sci. 15 (2016) 334–350, http://dx.doi.org/10.1039/C5PP00409H.
[22] D.J. Klionsky, K. Abdelmohsen, A. Abe, M.J. Abedin, H. Abeliovich, A. Acevedo Arozena, H. Adachi, C.M. Adams, P.D. Adams, K. Adeli, P.J. Adhihetty, S.G. Adler, G. Agam, R. Agarwal, M.K. Aghi, M. Agnello, P. Agostinis, P.V. Aguilar, J. Aguirre-Ghiso, E.M. Airoldi, S. Ait-Si-Ali, T. Akematsu, E.T. Akporiaye, M. Al-Rubeai, G.M. Albaiceta, C. Albanese, D. Albani, M.L. Albert, J. Aldudo, H. Algül, M. Alirezaei, I. Alloza, A. Almasan, M. Almonte-Beceril, E.S. Alnemri, C. Alonso, N. Altan-Bonnet, D.C. Altieri, S. Alvarez, L. Alvarez-Erviti, S. Alves, G. Amadoro, A. Amano, C. Amantini, S. Ambrosio, I. Amelio, A.O. Amer, M. Amessou, A. Amon, Z. An, F.A. Anania, S.U. Andersen, U.P. Andley, C.K. Andreadi, N. Andrieu-Abadie, A. Anel, D.K. Ann, S. Anoopkumar-Dukie, M. Antonioli, H. Aoki, N. Apostolova, S. Aquila, K. Aquilano, K. Araki, E. Arama, A. Aranda, J. Araya, A. Arcaro, E. Arias, H. Arimoto, A.R. Ariosa, J.L. Armstrong, T. Arnould, I. Arsov, K. Asanuma, V. Askanas, E. Asselin, R. Atarashi, S.S. Atherton, J.D. Atkin, L.D. Attardi, P. Auberger, G. Auburger, L. Aurelian, R. Autelli, L. Avagliano, M.L. Avantaggiati, L. Avrahami, S. Awale, N. Azad, T. Bachetti, J.M. Backer, D.-H. Bae, J. Bae, O.-N. Bae, S.H. Bae, E.H. Baehrecke, S.-H. Baek, S. Baghdiguian, A. Bagniewska-Zadworna, H. Bai, J. Bai, X.-Y. Bai, Y. Bailly, K.N. Balaji, W. Balduini, A. Ballabio, R. Balzan, R. Banerjee, G. Bánhegyi, H. Bao, B. Barbeau, M.D. Barrachina, E. Barreiro, B. Bartel, A. Bartolomé, D.C. Bassham, M.T. Bassi, R.C. Bast, A. Basu, M.T. Batista, H. Batoko, M. Battino, K. Bauckman, B.L. Baumgarner, K.U. Bayer, R. Beale, J.-F. Beaulieu, G.R. Beck, C. Becker, J.D. Beckham,

P.-A. Bédard, P.J. Bednarski, T.J. Begley, C. Behl, C. Behrends, G.M. Behrens, K.E. Behrns, E. Bejarano, A. Belaid, F. Belleudi, G. Bénard, G. Berchem, D. Bergamaschi, M. Bergami, B. Berkhout, L. Berliocchi, A. Bernard, M. Bernard, F. Bernassola, A. Bertolotti, A.S. Bess, S. Besteiro, S. Bettuzzi, S. Bhalla, S. Bhattacharyya, S.K. Bhutia, C. Biagosch, M.W. Bianchi, M. Biard-Piechaczyk, V. Billes, C. Bincoletto, B. Bingol, S.W. Bird, M. Bitoun, I. Bjedov, C. Blackstone, L. Blanc, G.A. Blanco, H.K. Blomhoff, E. Boada-Romero, S. Böckler, M. Boes, K. Boesze-Battaglia, L.H. Boise, A. Bolino, A. Boman, P. Bonaldo, M. Bordi, J. Bosch, L.M. Botana, J. Botti, G. Bou, M. Bouché, M. Bouchecareilh, M.-J. Boucher, M.E. Boulton, S.G. Bouret, P. Boya, M. Boyer-Guittaut, P.V. Bozhkov, N. Brady, V.M. Braga, C. Brancolini, G.H. Braus, J.M. Bravo-San Pedro, L.A. Brennan, E.H. Bresnick, P. Brest, D. Bridges, M.-A. Bringer, M. Brini, G.C. Brito, B. Brodin, P.S. Brookes, E.J. Brown, K. Brown, H.E. Broxmeyer, A. Bruhat, P.C. Brum, J.H. Brumell, N. Brunetti-Pierri, R.J. Bryson-Richardson, S. Buch, A.M. Buchan, H. Budak, D.V. Bulavin, S.J. Bultman, G. Bultynck, V. Bumbasirevic, Y. Burelle, R.E. Burke, M. Burmeister, P. Bütikofer, L. Caberlotto, K. Cadwell, M. Cahova, D. Cai, J. Cai, Q. Cai, S. Calatayud, N. Camougrand, M. Campanella, G.R. Campbell, M. Campbell, S. Campello, R. Candau, I. Caniggia, L. Cantoni, L. Cao, A.B. Caplan, M. Caraglia, C. Cardinali, S.M. Cardoso, J.S. Carew, L.A. Carleton, C.R. Carlin, S. Carloni, S.R. Carlsson, D. Carmona-Gutierrez, L.A. Carneiro, O. Carnevali, S. Carra, A. Carrier, B. Carroll, C. Casas, J. Casas, G. Cassinelli, P. Castets, S. Castro-Obregon, G. Cavallini, I. Ceccherini, F. Cecconi, A.I. Cederbaum, V. Ceña, S. Cenci, C. Cerella, D. Cervia, S. Cetrullo, H. Chaachouay, H.-J. Chae, A.S. Chagin, C.-Y. Chai, G. Chakrabarti, G. Chamilos, E.Y. Chan, M.T. Chan, D. Chandra, P. Chandra, C.-P. Chang, R.C.-C. Chang, T.Y. Chang, J.C. Chatham, S. Chatterjee, S. Chauhan, Y. Che, M.E. Cheetham, R. Cheluvappa, C.-J. Chen, G. Chen, G.-C. Chen, G. Chen, H. Chen, J.W. Chen, J.-K. Chen, M. Chen, M. Chen, P. Chen, Q. Chen, Q. Chen, S.-D. Chen, S. Chen, S.S.-L. Chen, W. Chen, W.-J. Chen, W.Q. Chen, W. Chen, X. Chen, Y.-H. Chen, Y.-G. Chen, Y. Chen, Y. Chen, Y. Chen, Y.-J. Chen, Y.-Q. Chen, Y. Chen, Z. Chen, Z. Chen, A. Cheng, C.H. Cheng, H. Cheng, H. Cheong, S. Cherry, J. Chesney, C.H.A. Cheung, E. Chevet, H.C. Chi, S.-G. Chi, F. Chiacchiera, H.-L. Chiang, R. Chiarelli, M. Chiariello, M. Chieppa, L.-S. Chin, M. Chiong, G.N. Chiu, D.-H. Cho, S.-G. Cho, W.C. Cho, Y.-Y. Cho, Y.-S. Cho, A.M. Choi, E.-J. Choi, E.-K. Choi, J. Choi, M.E. Choi, S.-I. Choi, T.-F. Chou, S. Chouaib, D. Choubey, V. Choubey, K.-C. Chow, K. Chowdhury, C.T. Chu, T.-H. Chuang, T. Chun, H. Chung, T. Chung, Y.-L. Chung, Y.-J. Chwae, V. Cianfanelli, R. Ciarcia, I.A. Ciechomska, M.R. Ciriolo, M. Cirone, S. Claerhout, M.J. Clague, J. Clària, P.G. Clarke, R. Clarke, E. Clementi, C. Cleyrat, M. Cnop, E.M. Coccia, T. Cocco, P. Codogno, J. Coers, E.E. Cohen, D. Colecchia, L. Coletto, N.S. Coll, E. Colucci-Guyon, S. Comincini, M. Condello, K.L. Cook, G.H. Coombs, C.D. Cooper, J.M. Cooper, I. Coppens, M.T. Corasaniti, M. Corazzari, R. Corbalan, E. Corcelle-Termeau, M.D. Cordero, C. Corral-Ramos, O. Corti, A. Cossarizza, P. Costelli, S. Costes, S.L. Cotman, A. Coto-Montes, S. Cottet, E. Couve, L.R. Covey, L.A. Cowart, J.S. Cox, F.P. Coxon, C.B. Coyne, M.S. Cragg, R.J. Craven, T. Crepaldi, J.L. Crespo, A. Criollo, V. Crippa, M.T. Cruz, A.M. Cuervo, J.M. Cuezva, T. Cui, P.R. Cutillas, M.J. Czaja, M.F. Czyzyk-Krzeska, R.K. Dagda, U. Dahmen, C. Dai, W. Dai, Y. Dai, K.N. Dalby, L. Dalla Valle, G. Dalmasso, M. D'Amelio, M. Damme, A. Darfeuille-Michaud, C. Dargemont, V.M. Darley-Usmar, S. Dasarathy, B. Dasgupta, S. Dash, C.R. Dass, H.M. Davey, L.M. Davids, D. Dávila, R.J. Davis, T.M. Dawson, V.L. Dawson, P. Daza, J. de Belleroche, P. de Figueiredo, R.C.B.Q. de Figueiredo, J. de la Fuente, L. De Martino, A. De Matteis, G.R. De Meyer, A. De Milito, M. De Santi, W. de Souza, V. De Tata, D. De Zio, J. Debnath, R. Dechant, J.-P. Decuypere, S. Deegan, B. Dehay, B. Del Bello, D.P. Del Re, R. Delage-Mourroux, L.M. Delbridge, L. Deldicque, E. Delorme-Axford, Y. Deng, J. Dengjel, M. Denizot, P. Dent, C.J. Der, V. Deretic, B. Derrien, E. Deutsch, T.P. Devarenne, R.J. Devenish, S. Di Bartolomeo, N. Di Daniele, F. Di Domenico, A. Di Nardo, S. Di Paola, A. Di Pietro, L. Di Renzo, A. Di Antonio, G. Díaz-Araya, I. Díaz-Laviada, M.T. Diaz-Meco, J. Diaz-Nido, C.A. Dickey, R.C. Dickson, M. Diederich, P. Digard, I. Dikic, S.P. Dinesh-Kumar, C. Ding, W.-X. Ding, Z. Ding, L. Dini, J.H. Distler, A. Diwan, M. Djavaheri-Mergny, K. Dmytruk, R.C. Dobson, V. Doetsch, K. Dokladny, S. Dokudovskaya, M. Donadelli, X.C. Dong, X. Dong, Z. Dong, T.M. Donohue, K.S. Doran, G. D'Orazi, G.W. Dorn, V. Dosenko, S. Dridi, L. Drucker, J. Du, L.-L. Du, L. Du, A. du Toit, P. Dua, L. Duan, P. Duann, V.K. Dubey, M.R. Duchen, M.A. Duchosal, H. Duez, I. Dugail, V.I. Dumit, M.C. Duncan, E.A. Dunlop, W.A. Dunn, N. Dupont, L. Dupuis, R.V. Durán, T.M. Durcan, S. Duvezin-Caubet, U. Duvvuri, V. Eapen, D. Ebrahimi-Fakhari, A. Echard, L. Eckhart, C.L. Edelstein, A.L. Edinger, L. Eichinger, T. Eisenberg, A. Eisenberg-Lerner, N.T. Eissa, W.S. El-Deiry, V. El-Khoury, Z. Elazar, H. Eldar-Finkelman, C.J. Elliott, E. Emanuele, U. Emmenegger, N. Engedal, A.-M. Engelbrecht, S. Engelender, J.M. Enserink, R. Erdmann, J. Erenpreisa, R. Eri, J.L. Eriksen, A. Erman, R. Escalante, E.-L. Eskelinen, L. Espert, L. Esteban-Martínez, T.J. Evans, M. Fabri, G. Fabrias, C. Fabrizi, A. Facchiano, N.J. Færgeman, A. Faggioni, W.D. Fairlie, C. Fan, D. Fan, J. Fan, S. Fang, M. Fanto, A. Fanzani, T. Farkas, M. Faure, F.B. Favier, H. Fearnhead, M. Federici, E. Fei, T.C. Felizardo, H. Feng, Y. Feng, Y. Feng, T.A. Ferguson, Á.F. Fernández, M.G. Fernandez-Barrena, J.C. Fernandez-Checa, A. Fernández-López, M.E. Fernandez-Zapico, O. Feron, E. Ferraro, C.V. Ferreira-Halder, L. Fesus, R. Feuer, F.C. Fiesel, E.C. Filippi-Chiela, G. Filomeni, G.M. Fimia, J.H. Fingert, S. Finkbeiner, T. Finkel, F. Fiorito, P.B. Fisher, M. Flajolet, F. Flamigni, O. Florey, S. Florio, R.A. Floto, M. Folini, C. Follo, E.A. Fon, F. Fornai, F. Fortunato, A. Fraldi, R. Franco, A. Francois, A. François, L.B. Frankel, I.D. Fraser, N. Frey, D.G. Freyssenet, C. Frezza, S.L. Friedman, D.E. Frigo, D. Fu, J.M. Fuentes, J. Fueyo, Y. Fujitani, Y. Fujiwara, M. Fujiya, M. Fukuda, S. Fulda, C. Fusco, B. Gabryel, M. Gaestel, P. Gailly, M. Gajewska, S. Galadari, G. Galili, I. Galindo, M.F. Galindo, G. Galliciotti, L. Galluzzi, L. Galluzzi, V. Galy, N. Gammoh, S. Gandy, A.K. Ganesan, S. Ganesan, I.G. Ganley, M. Gannagé, F.-B. Gao, F. Gao, J.-X. Gao, L. García Nannig, E. García Véscovi, M. Garcia-Macía, C. Garcia-Ruiz, A.D. Garg, P.K. Garg, R. Gargini, N.C. Gassen, D. Gatica, E. Gatti, J. Gavard, E. Gavathiotis, L. Ge, P. Ge, S. Ge, P.-W. Gean, V. Gelmetti, A.A. Genazzani, J. Geng, P. Genschik, L. Gerner, J.E. Gestwicki, D.A. Gewirtz, S. Ghavami, E. Ghigo, D. Ghosh, A.M. Giammarioli, F. Giampieri, C. Giampietri, A. Giatromanolaki, D.J. Gibbings, L. Gibellini, S.B. Gibson, V. Ginet, A. Giordano, F. Giorgini, E. Giovannetti, S.E. Girardin, S. Gispert, S. Giuliano, C.L. Gladson, A. Glavic, M. Gleave, N. Godefroy, R.M. Gogal, K. Gokulan, G.H. Goldman, D. Goletti, M.S. Goligorsky, A.V. Gomes, L.C. Gomes, H. Gomez, C. Gomez-Manzano, R. Gómez-Sánchez, D.A. Gonçalves, E. Goncu, Q. Gong, C. Gongora, C.B. Gonzalez, P. Gonzalez-Alegre, P. Gonzalez-Cabo, R.A. González-Polo, I.S. Goping, C. Gorbea, N.V. Gorbunov, D.R. Goring, A.M. Gorman, S.M. Gorski, S. Goruppi, S. Goto-Yamada, C. Gotor, R.A. Gottlieb, I. Gozes, D. Gozuacik, Y. Graba, M. Graef, G.E. Granato, G.D. Grant, S. Grant, G.L. Gravina, D.R. Green, A. Greenhough, M.T. Greenwood, B. Grimaldi, F. Gros, C. Grose, J.-F. Groulx, F. Gruber, P. Grumati, T. Grune, J.-L. Guan, K.-L. Guan, B. Guerra, C. Guillen, K. Gulshan, J. Gunst, C. Guo, L. Guo, M. Guo, W. Guo, X.-G. Guo, A.A. Gust, Å.B. Gustafsson, E. Gutierrez, M.G. Gutierrez, H.-S. Gwak, A. Haas, J.E. Haber, S. Hadano, M. Hagedorn, D.R. Hahn, A.J. Halayko, A. Hamacher-Brady, K. Hamada, A. Hamai, A. Hamann, M. Hamasaki, I. Hamer, Q. Hamid, E.M. Hammond, F. Han, W. Han, J.T. Handa, J.A. Hanover, M. Hansen, M. Harada, L. Harhaji-Trajkovic, J.W. Harper, A.H. Harrath, A.L. Harris, J. Harris, U. Hasler, P. Hasselblatt, K. Hasui, R.G. Hawley, T.S. Hawley, C. He, C.Y. He, F. He, G. He, R.-R. He, X.-H. He, Y.-W. He, Y.-Y. He, J.K. Heath, M.-J. Hébert, R.A. Heinzen, G.V. Helgason, M. Hensel, E.P. Henske, C. Her, P.K. Herman, A. Hernández, C. Hernandez, S. Hernández-Tiedra, C. Hetz, P.R. Hiesinger, K. Higaki, S. Hilfiker, B.G. Hill, J.A. Hill, W.D. Hill, K. Hino, D. Hofius, P. Hofman, G.U. Höglinger, J. Höhfeld, M.K. Holz, Y. Hong, D.A. Hood, J.J. Hoozemans, T. Hoppe, C. Hsu, C.-Y. Hsu, L.-C. Hsu, D. Hu, G. Hu, H.-M. Hu, H. Hu, M.C. Hu, Y.-C. Hu, Z.-W. Hu, F. Hua, Y. Hua, C. Huang, H.-L. Huang, K.-H. Huang, K.-Y. Huang, S. Huang, S. Huang, W.-P. Huang, Y.-R. Huang, Y. Huang, Y. Huang, T.B. Huber, P. Huebbe, W.-K. Huh, J.J. Hulmi, G.M. Hur, J.H. Hurley, Z. Husak, S.N. Hussain, S. Hussain, J.J. Hwang, S. Hwang, T.I. Hwang, A. Ichihara, Y. Imai, C. Imbriano, M. Inomata, T. Into, V. Iovane, J.L. Iovanna, R.V. Iozzo, N.Y. Ip, J.E. Irazoqui, P. Iribarren, Y. Isaka, A.J. Isakovic, H. Ischiropoulos, J.S. Isenberg, M. Ishaq, H. Ishida, I. Ishii, J.E. Ishmael, C. Isidoro, K. Isobe, E. Isono, S. Issazadeh-Navikas, K. Itahana, E. Itakura, A.I. Ivanov, A.K.V. Iyer, J.M. Izquierdo, Y. Izumi, V. Izzo, M. Jäättelä, N. Jaber, D.J. Jackson, W.T. Jackson, T.G. Jacob, T.S. Jacques, C. Jagannath, A. Jain, N.R. Jana, B.K. Jang, A. Jani, B. Janji, P.R. Jannig, P.J. Jansson, S. Jean, M. Jendrach, J.-H. Jeon, N. Jessen, E.-B. Jeung, K. Jia, L. Jia, H. Jiang, H. Jiang, L. Jiang, T. Jiang, X. Jiang, X. Jiang, X. Jiang, Y. Jiang, Y. Jiang, A. Jiménez, C. Jin, H. Jin, L. Jin, M. Jin, S. Jin, U.K. Jinwal, E.-K. Jo, T. Johansen, D.E. Johnson, G.V. Johnson, J.D. Johnson, E. Jonasch, C. Jones, L.A. Joosten, J. Jordan, A.-M. Joseph, B. Joseph, A.M. Joubert, D. Ju, J. Ju, H.-F. Juan, K. Juenemann, G. Juhász, H.S. Jung, J.U. Jung, Y.-K. Jung, H. Jungbluth, M.J. Justice, B. Jutten, N.O. Kaakoush, K. Kaarniranta, A. Kaasik, T. Kabuta, B. Kaeffer, K. Kågedal, A. Kahana, S. Kajimura, O. Kakhlon, M. Kalia, D.V. Kalvakolanu, Y. Kamada, K. Kambas, V.O. Kaminskyy, H.H. Kampinga, M. Kandouz, C. Kang, R. Kang, T.-C. Kang, T. Kanki, T.-D. Kanneganti, H. Kanno, A.G. Kanthasamy, M. Kantorow, M. Kaparakis-Liaskos, O. Kapuy, V. Karantza, M.R. Karim, P. Karmakar, A. Kaser, S. Kaushik, T. Kawula, A.M. Kaynar, P.-Y. Ke, Z.-J. Ke, J.H. Kehrl, K.E. Keller, J.K. Kemper, A.K. Kenworthy, O. Kepp, A. Kern, S. Kesari, D. Kessel, R. Ketteler, I. do C. Kettelhut, B. Khambu, M.M. Khan, V.K. Khandelwal, S. Khare, J.G. Kiang, A.A. Kiger, A. Kihara, A.L. Kim, C.H. Kim, D.R. Kim, D.-H. Kim, E.K. Kim, H.Y. Kim, H.-R. Kim, J.-S. Kim, J.H. Kim, J.C. Kim, J.H. Kim, K.W. Kim, M.D. Kim, M.-M. Kim, P.K. Kim, S.W. Kim, S.-Y. Kim, Y.-S. Kim, Y. Kim, A. Kimchi, A.C. Kimmelman, T. Kimura, J.S. King, K. Kirkegaard, V. Kirkin, L.A. Kirshenbaum, S. Kishi, Y. Kitajima, K. Kitamoto, Y. Kitaoka, K. Kitazato, R.A. Kley, W.T. Klimecki, M. Klinkenberg, J. Klucken, H. Knævelsrud, E. Knecht, L. Knuppertz, J.-L. Ko, S. Kobayashi, J.C. Koch, C. Koechlin-Ramonatxo, U. Koenig, Y.H. Koh, K. Köhler, S.D. Kohlwein, M. Koike, M. Komatsu, E. Kominami, D. Kong, H.J. Kong, E.G. Konstantakou, B.T. Kopp, T. Korcsmaros, L. Korhonen, V.I. Korolchuk, N.V. Koshkina, Y. Kou, M.I. Koukourakis, C. Koumenis, A.L. Kovács, T. Kovács, W.J. Kovacs, D. Koya, C. Kraft, D. Krainc, H. Kramer, T. Kravic-Stevovic, W. Krek, C. Kretz-Remy, R. Krick, M. Krishnamurthy, J. Kriston-Vizi, G. Kroemer, M.C. Kruer, R. Kruger, N.T. Ktistakis, K. Kuchitsu, C. Kuhn, A.P. Kumar, A. Kumar, A. Kumar, D. Kumar, D. Kumar, R. Kumar, S. Kumar, M. Kundu, H.-J. Kung, A. Kuno, S.-H. Kuo, J. Kuret, T. Kurz, T. Kwok, T.K. Kwon, Y.T. Kwon, I. Kyrmizi, A.R. La Spada, F. Lafont, T. Lahm, A. Lakkaraju, T. Lam, T. Lamark, S. Lancel, T.H. Landowski, D.J. Lane, J.D. Lane, C. Lanzi, P. Lapaquette, L.R. Lapierre, J. Laporte, J. Laukkarinen, G.W. Laurie, S. Lavandero, L. Lavie, M.J. LaVoie, B.Y.K. Law, H.K. Law, K.B. Law, R. Layfield, P.A. Lazo, L. Le Cam, K.G. Le Roch, H. Le Stunff, V. Leardkamolkarn, M. Lecuit, B.-H. Lee, C.-H. Lee, E.F. Lee, G.M. Lee, H.-J. Lee, H. Lee, J.K. Lee, J. Lee, J. Lee, J.H. Lee, M. Lee, M.-S. Lee, P.J. Lee, S.W. Lee, S.-J. Lee, S.-J. Lee, S.Y. Lee, S.H. Lee, S.S. Lee, S.-J. Lee, S. Lee, Y.-R. Lee, Y.J. Lee, Y.H. Lee, C. Leeuwenburgh, S. Lefort, R. Legouis, J. Lei, Q.-Y. Lei, D.A. Leib, G. Leibowitz, I. Lekli, S.D. Lemaire, J.J. Lemasters, M.K. Lemberg, A. Lemoine, S. Leng, G. Lenz, P. Lenzi, L.O. Lerman, D. Lettieri Barbato, J.I.-J. Leu, H.Y. Leung, B. Levine, P.A. Lewis, F. Lezoualc'h, C. Li, F. Li, F.-J. Li, J. Li, K. Li, L. Li, M. Li, M. Li, Q. Li, R. Li, S. Li, W. Li, W. Li, X. Li, Y. Li, J. Lian, C. Liang, Q. Liang, Y. Liao, J. Liberal, P.P. Liberski, P. Lie, A.P. Lieberman, H.J. Lim, K.-L. Lim, K. Lim, R.T. Lima, C.-S. Lin, C.-F. Lin, F. Lin, F. Lin, F.-C. Lin, K. Lin, K.-H. Lin, P.-H. Lin, T. Lin, W.-W. Lin, Y.-S. Lin, Y. Lin, R. Linden, D. Lindholm, L.M. Lindqvist, P. Lingor, A. Linkermann, L.A. Liotta, M.M. Lipinski, V.A. Lira, M.P. Lisanti, P.B. Liton, B. Liu, C. Liu, C.-F. Liu, F. Liu, H.-J. Liu, J. Liu, J.-J. Liu, J.-L. Liu, K. Liu, L. Liu, L. Liu, Q. Liu, R.-Y. Liu, S. Liu, S. Liu, W. Liu, X.-D. Liu, X. Liu, X.-H. Liu, X. Liu, X. Liu, X. Liu, Y. Liu, Y. Liu, Z. Liu, Z. Liu, J.P. Liuzzi, G. Lizard, M. Ljujic, I.J. Lodhi, S.E. Logue, B.L. Lokeshwar, Y.C. Long, S. Lonial, B. Loos, C. López-Otín, C. López-Vicario, M. Lorente, P.L. Lorenzi, P. Lõrincz, M. Los, M.T. Lotze, P.E. Lovat, B. Lu, B. Lu, J. Lu, Q. Lu, S.-M. Lu, S. Lu, Y. Lu, F. Luciano, S. Luckhart, J.M. Lucocq, P. Ludovico, A. Lugea, N.W. Lukacs, J.J. Lum, A.H. Lund, H. Luo, J. Luo, S. Luo, C. Luparello, T. Lyons, J. Ma, Y. Ma, Y. Ma, Z. Ma, J. Machado, G.M. Machado-Santelli, F. Macian, G.C. MacIntosh, J.P. MacKeigan, K.F. Macleod, J.D. MacMicking, L.A. MacMillan-Crow, F. Madeo, M. Madesh, J. Madrigal-Matute, A. Maeda, T. Maeda, G. Maegawa, E. Maellaro, H. Maes, M. Magariños, K. Maiese, T.K. Maiti, L. Maiuri, M.C. Maiuri, C.G. Maki, R. Malli, W. Malorni, A. Maloyan, F. Mami-Chouaib, N. Man, J.D. Mancias, E.-M. Mandelkow, M.A. Mandell, A.A. Manfredi, S.N. Manié, C. Manzoni, K. Mao, Z.

Mao, Z.-W. Mao, P. Marambaud, A.M. Marconi, Z. Marelja, G. Marfe, M. Margeta, E. Margittai, M. Mari, F.V. Mariani, C. Marin, S. Marinelli, G. Mariño, I. Markovic, R. Marquez, A.M. Martelli, S. Martens, K.R. Martin, S.J. Martin, S. Martin, M.A. Martin-Acebes, P. Martín-Sanz, C. Martinand-Mari, W. Martinet, J. Martinez, N. Martinez-Lopez, U. Martinez-Outschoorn, M. Martínez-Velázquez, M. Martinez-Vicente, W.K. Martins, H. Mashima, J.A. Mastrianni, G. Matarese, P. Matarrese, R. Mateo, S. Matoba, N. Matsumoto, T. Matsushita, A. Matsuura, T. Matsuzawa, M.P. Mattson, S. Matus, N. Maugeri, C. Mauvezin, A. Mayer, D. Maysinger, G.D. Mazzolini, M.K. McBrayer, K. McCall, C. McCormick, G.M. McInerney, S.C. McIver, S. McKenna, J.J. McMahon, I.A. McNeish, F. Mechta-Grigoriou, J.P. Medema, D.L. Medina, K. Megyeri, M. Mehrpour, J.L. Mehta, Y. Mei, U.-C. Meier, A.J. Meijer, A. Meléndez, G. Melino, S. Melino, E.J.T. de Melo, M.A. Mena, M.D. Meneghini, J.A. Menendez, R. Menezes, L. Meng, L. Meng, S. Meng, R. Menghini, A.S. Menko, R.F. Menna-Barreto, M.B. Menon, M.A. Meraz-Ríos, G. Merla, L. Merlini, A.M. Merlot, A. Meryk, S. Meschini, J.N. Meyer, M. Mi, C.-Y. Miao, L. Micale, S. Michaeli, C. Michiels, A.R. Migliaccio, A.S. Mihailidou, D. Mijaljica, K. Mikoshiba, E. Milan, L. Miller-Fleming, G.B. Mills, I.G. Mills, G. Minakaki, B.A. Minassian, X.-F. Ming, F. Minibayeva, E.A. Minina, J.D. Mintern, S. Minucci, A. Miranda-Vizuete, C.H. Mitchell, S. Miyamoto, K. Miyazawa, N. Mizushima, K. Mnich, B. Mograbi, S. Mohseni, L.F. Moita, M. Molinari, M. Molinari, A.B. Møller, B. Mollereau, F. Mollinedo, M. Mongillo, M.M. Monick, S. Montagnaro, C. Montell, D.J. Moore, M.N. Moore, R. Mora-Rodriguez, P.I. Moreira, E. Morel, M.B. Morelli, S. Moreno, M.J. Morgan, A. Moris, Y. Moriyasu, J.L. Morrison, L.A. Morrison, E. Morselli, J. Moscat, P.L. Moseley, S. Mostowy, E. Motori, D. Mottet, J.C. Mottram, C.E.-H. Moussa, V.E. Mpakou, H. Mukhtar, J.M. Mulcahy Levy, S. Muller, R. Muñoz-Moreno, C. Muñoz-Pinedo, C. Münz, M.E. Murphy, J.T. Murray, A. Murthy, I.U. Mysorekar, I.R. Nabi, M. Nabissi, G.A. Nader, Y. Nagahara, Y. Nagai, K. Nagata, A. Nagelkerke, P. Nagy, S.R. Naidu, S. Nair, H. Nakano, H. Nakatogawa, M. Nanjundan, G. Napolitano, N.I. Naqvi, R. Nardacci, D.P. Narendra, M. Narita, A.C. Nascimbeni, R. Natarajan, L.C. Navegantes, S.T. Nawrocki, T.Y. Nazarko, V.Y. Nazarko, T. Neill, L.M. Neri, M.G. Netea, R.T. Netea-Maier, B.M. Neves, P.A. Ney, I.P. Nezis, H.T. Nguyen, H.P. Nguyen, A.-S. Nicot, H. Nilsen, P. Nilsson, M. Nishimura, I. Nishino, M. Niso-Santano, H. Niu, R.A. Nixon, V.C. Njar, T. Noda, A.A. Noegel, E.M. Nolte, E. Norberg, K.K. Norga, S.K. Noureini, S. Notomi, L. Notterpek, K. Nowikovsky, N. Nukina, T. Nürnberger, V.B. O'Donnell, T. O'Donovan, P.J. O'Dwyer, I. Oehme, C.L. Oeste, M. Ogawa, B. Ogretmen, Y. Ogura, Y.J. Oh, M. Ohmuraya, T. Ohshima, R. Ojha, K. Okamoto, T. Okazaki, F.J. Oliver, K. Ollinger, S. Olsson, D.P. Orban, P. Ordonez, I. Orhon, L. Orosz, E.J. O'Rourke, H. Orozco, A.L. Ortega, E. Ortona, L.D. Osellame, J. Oshima, S. Oshima, H.D. Osiewacz, T. Otomo, K. Otsu, J.J. Ou, T.F. Outeiro, D. Ouyang, H. Ouyang, M. Overholtzer, M.A. Ozbun, P.H. Ozdinler, B. Ozpolat, C. Pacelli, P. Paganetti, G. Page, G. Pages, U. Pagnini, B. Pajak, S.C. Pak, K. Pakos-Zebrucka, N. Pakpour, Z. Palková, F. Palladino, K. Pallauf, N. Pallet, M. Palmieri, S.R. Paludan, C. Palumbo, S. Palumbo, O. Pampliega, H. Pan, W. Pan, T. Panaretakis, A. Pandey, A. Pantazopoulou, Z. Papackova, D.L. Papademetrio, I. Papassideri, A. Papini, N. Parajuli, J. Pardo, V.V. Parekh, G. Parenti, J.-I. Park, J. Park, O.K. Park, R. Parker, R. Parlato, J.B. Parys, K.R. Parzych, J.-M. Pasquet, B. Pasquier, K.B. Pasumarthi, D. Patschan, C. Patterson, S. Pattingre, S. Pattison, A. Pause, H. Pavenstädt, F. Pavone, Z. Pedrozo, F.J. Peña, M.A. Peñalva, M. Pende, J. Peng, F. Penna, J.M. Penninger, A. Pensalfini, S. Pepe, G.J. Pereira, P.C. Pereira, V. Pérez-de la Cruz, M.E. Pérez-Pérez, D. Pérez-Rodríguez, D. Pérez-Sala, C. Perier, A. Perl, D.H. Perlmutter, I. Perrotta, S. Pervaiz, M. Pesonen, J.E. Pessin, G.J. Peters, M. Petersen, I. Petrache, B.J. Petrof, G. Petrovski, J.M. Phang, M. Piacentini, M. Pierdominici, P. Pierre, V. Pierrefite-Carle, F. Pietrocola, F.X. Pimentel-Muiños, M. Pinar, B. Pineda, R. Pinkas-Kramarski, M. Pinti, P. Pinton, B. Piperdi, J.M. Piret, L.C. Platanias, H.W. Platta, E.D. Plowey, S. Pöggeler, M. Poirot, P. Polčic, A. Poletti, A.H. Poon, H. Popelka, B. Popova, I. Poprawa, S.M. Poulose, J. Poulton, S.K. Powers, T. Powers, M. Pozuelo-Rubio, K. Prak, R. Prange, M. Prescott, M. Priault, S. Prince, R.L. Proia, T. Proikas-Cezanne, H. Prokisch, V.J. Promponas, K. Przyklenk, R. Puertollano, S. Pugazhenthi, L. Puglielli, A. Pujol, J. Puyal, D. Pyeon, X. Qi, W. Qian, Z.-H. Qin, Y. Qiu, Z. Qu, J. Quadrilatero, F. Quinn, N. Raben, H. Rabinowich, F. Radogna, M.J. Ragusa, M. Rahmani, K. Raina, S. Ramanadham, R. Ramesh, A. Rami, S. Randall-Demllo, F. Randow, H. Rao, V.A. Rao, B.B. Rasmussen, T.M. Rasse, E.A. Ratovitski, P.-E. Rautou, S.K. Ray, B. Razani, B.H. Reed, F. Reggiori, M. Rehm, A.S. Reichert, T. Rein, D.J. Reiner, E. Reits, J. Ren, X. Ren, M. Renna, J.E. Reusch, J.L. Revuelta, L. Reyes, A.R. Rezaie, R.I. Richards, D.R. Richardson, C. Richetta, M.A. Riehle, B.H. Rihn, Y. Rikihisa, B.E. Riley, G. Rimbach, M.R. Rippo, K. Ritis, F. Rizzi, E. Rizzo, P.J. Roach, J. Robbins, M. Roberge, G. Roca, M.C. Roccheri, S. Rocha, C.M. Rodrigues, C.I. Rodríguez, S.R. de Cordoba, N. Rodriguez-Muela, J. Roelofs, V.V. Rogov, T.T. Rohn, B. Rohrer, D. Romanelli, L. Romani, P.S. Romano, M.I.G. Roncero, J.L. Rosa, A. Rosello, K.V. Rosen, P. Rosenstiel, M. Rost-Roszkowska, K.A. Roth, G. Roué, M. Rouis, K.M. Rouschop, D.T. Ruan, D. Ruano, D.C. Rubinsztein, E.B. Rucker, A. Rudich, E. Rudolf, R. Rudolf, M.A. Ruegg, C. Ruiz-Roldan, A.A. Ruparelia, P. Rusmini, D.W. Russ, G.L. Russo, G. Russo, R. Russo, T.E. Rusten, V. Ryabovol, K.M. Ryan, S.W. Ryter, D.M. Sabatini, M. Sacher, C. Sachse, M.N. Sack, J. Sadoshima, P. Saftig, R. Sagi-Eisenberg, S. Sahni, P. Saikumar, T. Saito, T. Saitoh, K. Sakakura, M. Sakoh-Nakatogawa, Y. Sakuraba, M. Salazar-Roa, P. Salomoni, A.K. Saluja, P.M. Salvaterra, R. Salvioli, A. Samali, A.M. Sanchez, J.A. Sánchez-Alcázar, R. Sanchez-Prieto, M. Sandri, M.A. Sanjuan, S. Santaguida, L. Santambrogio, G. Santoni, C.N. dos Santos, S. Saran, M. Sardiello, G. Sargent, P. Sarkar, S. Sarkar, M.R. Sarrias, M.M. Sarwal, C. Sasakawa, M. Sasaki, M. Sass, K. Sato, M. Sato, J. Satriano, N. Savaraj, S. Saveljeva, L. Schaefer, U.E. Schaible, M. Scharl, H.M. Schatzl, R. Schekman, W. Scheper, A. Schiavi, H.M. Schipper, H. Schmeisser, J. Schmidt, I. Schmitz, B.E. Schneider, E.M. Schneider, J.L. Schneider, E.A. Schon, M.J. Schönenberger, A.H. Schönthal, D.F. Schorderet, B. Schröder, S. Schuck, R.J. Schulze, M. Schwarten, T.L. Schwarz, S. Sciarretta, K. Scotto, A.I. Scovassi, R.A. Screaton, M. Screen, H. Seca, S. Sedej, L. Segatori, N. Segev, P.O. Seglen, J.M. Seguí-Simarro, J. Segura-Aguilar, E. Seki, C. Sell, I. Selliez, C.F. Semenkovich, G.L. Semenza, U. Sen, A.L. Serra, A. Serrano-Puebla, H. Sesaki, T. Setoguchi, C. Settembre, J.J. Shacka, A.N. Shajahan-Haq, I.M. Shapiro, S. Sharma, H. She, C.-K.J. Shen, C.-C. Shen, H.-M. Shen, S. Shen, W. Shen, R. Sheng, X. Sheng, Z.-H. Sheng, T.G. Shepherd, J. Shi, Q. Shi, Q. Shi, Y. Shi, S. Shibutani, K. Shibuya, Y. Shidoji, J.-J. Shieh, C.-M. Shih, Y. Shimada, S. Shimizu, D.W. Shin, M.L. Shinohara, M. Shintani, T. Shintani, T. Shioi, K. Shirabe, R. Shiri-Sverdlov, O. Shirihai, G.C. Shore, C.-W. Shu, D. Shukla, A.A. Sibirny, V. Sica, C.J. Sigurdson, E.M. Sigurdsson, P.S. Sijwali, B. Sikorska, W.A. Silveira, S. Silvente-Poirot, G.A. Silverman, J. Simak, T. Simmet, A.K. Simon, H.-U. Simon, C. Simone, M. Simons, A. Simonsen, R. Singh, S.V. Singh, S.K. Singh, D. Sinha, S. Sinha, F.A. Sinicrope, A. Sirko, K. Sirohi, B.J. Sishi, A. Sittler, P.M. Siu, E. Sivridis, A. Skwarska, R. Slack, I. Slaninová, N. Slavov, S.S. Smaili, K.S. Smalley, D.R. Smith, S.J. Soenen, S.A. Soleimanpour, A. Solhaug, K. Somasundaram, J.H. Son, A. Sonawane, C. Song, F. Song, H.K. Song, J.-X. Song, W. Song, K.Y. Soo, A.K. Sood, T.W. Soong, V. Soontornniyomkij, M. Sorice, F. Sotgia, D.R. Soto-Pantoja, A. Sotthibundhu, M.J. Sousa, H.P. Spaink, P.N. Span, A. Spang, J.D. Sparks, P.G. Speck, S.A. Spector, C.D. Spies, W. Springer, D.S. Clair, A. Stacchiotti, B. Staels, M.T. Stang, D.T. Starczynowski, P. Starokadomskyy, C. Steegborn, J.W. Steele, L. Stefanis, J. Steffan, C.M. Stellrecht, H. Stenmark, T.M. Stepkowski, S.T. Stern, C. Stevens, B.R. Stockwell, V. Stoka, Z. Storchova, B. Stork, V. Stratoulias, D.J. Stravopodis, P. Strnad, A.M. Strohecker, A.-L. Ström, P. Stromhaug, J. Stulik, Y.-X. Su, Z. Su, C.S. Subauste, S. Subramaniam, C.M. Sue, S.W. Suh, X. Sui, S. Sukseree, D. Sulzer, F.-L. Sun, J. Sun, J. Sun, S.-Y. Sun, Y. Sun, Y. Sun, Y. Sun, V. Sundaramoorthy, J. Sung, H. Suzuki, K. Suzuki, N. Suzuki, T. Suzuki, Y.J. Suzuki, M.S. Swanson, C. Swanton, K. Swärd, G. Swarup, S.T. Sweeney, P.W. Sylvester, Z. Szatmari, E. Szegezdi, P.W. Szlosarek, H. Taegtmeyer, M. Tafani, E. Taillebourg, S.W. Tait, K. Takacs-Vellai, Y. Takahashi, S. Takáts, G. Takemura, N. Takigawa, N.J. Talbot, E. Tamagno, J. Tamburini, C.-P. Tan, L. Tan, M.L. Tan, M. Tan, Y.-J. Tan, K. Tanaka, M. Tanaka, D. Tang, D. Tang, G. Tang, I. Tanida, K. Tanji, B.A. Tannous, J.A. Tapia, I. Tasset-Cuevas, M. Tatar, I. Tavassoly, N. Tavernarakis, A. Taylor, G.S. Taylor, G.A. Taylor, J.P. Taylor, M.J. Taylor, E.V. Tchetina, A.R. Tee, F. Teixeira-Clerc, S. Telang, T. Tencomnao, B.-B. Teng, R.-J. Teng, F. Terro, G. Tettamanti, A.L. Theiss, A.E. Theron, K.J. Thomas, M.P. Thomé, P.G. Thomes, A. Thorburn, J. Thorner, T. Thum, M. Thumm, T.L. Thurston, L. Tian, A. Till, J.P. Ting, V.I. Titorenko, L. Toker, S. Toldo, S.A. Tooze, I. Topisirovic, M.L. Torgersen, L. Torosantucci, A. Torriglia, M.R. Torrisi, C. Tournier, R. Towns, V. Trajkovic, L.H. Travassos, G. Triola, D.N. Tripathi, D. Trisciuoglio, R. Troncoso, I.P. Trougakos, A.C. Truttmann, K.-J. Tsai, M.P. Tschan, Y.-H. Tseng, T. Tsukuba, A. Tsung, A.S. Tsvetkov, S. Tu, H.-Y. Tuan, M. Tucci, D.A. Tumbarello, B. Turk, V. Turk, R.F. Turner, A.A. Tveita, S.C. Tyagi, M. Ubukata, Y. Uchiyama, A. Udelnow, T. Ueno, M. Umekawa, R. Umemiya-Shirafuji, B.R. Underwood, C. Ungermann, R.P. Ureshino, R. Ushioda, V.N. Uversky, N.L. Uzcátegui, T. Vaccari, M.I. Vaccaro, L. Váchová, H. Vakifahmetoglu-Norberg, R. Valdor, E.M. Valente, F. Vallette, A.M. Valverde, G. Van den Berghe, L. Van Den Bosch, G.R. van den Brink, F.G. van der Goot, I.J. van der Klei, L.J. van der Laan, W.G. van Doorn, M. van Egmond, K.L. van Golen, L. Van Kaer, M. van Lookeren Campagne, P. Vandenabeele, W. Vandenberghe, I. Vanhorebeek, I. Varela-Nieto, M.H. Vasconcelos, R. Vasko, D.G. Vavvas, I. Vega-Naredo, G. Velasco, A.D. Velentzas, P.D. Velentzas, T. Vellai, E. Vellenga, M.H. Vendelbo, K. Venkatachalam, N. Ventura, S. Ventura, P.S. Veras, M. Verdier, B.G. Vertessy, A. Viale, M. Vidal, H.L.A. Vieira, R.D. Vierstra, N. Vigneswaran, N. Vij, M. Vila, M. Villar, V.H. Villar, J. Villarroya, C. Vindis, G. Viola, M.T. Viscomi, G. Vitale, D.T. Vogl, O.V. Voitsekhovskaja, C. von Haefen, K. von Schwarzenberg, D.E. Voth, V. Vouret-Craviari, K. Vuori, J.M. Vyas, C. Waeber, C.L. Walker, M.J. Walker, J. Walter, L. Wan, X. Wan, B. Wang, C. Wang, C.-Y. Wang, C. Wang, C. Wang, C. Wang, D. Wang, F. Wang, F. Wang, G. Wang, H. Wang, H. Wang, H.-G. Wang, H. Wang, H.-D. Wang, J. Wang, J. Wang, M. Wang, M.-Q. Wang, P.-Y. Wang, P. Wang, R.C. Wang, S. Wang, T.-F. Wang, X. Wang, X. Wang, X.-W. Wang, X. Wang, X. Wang, Y. Wang, Y. Wang, Y. Wang, Y.-J. Wang, Y. Wang, Y. Wang, Y.T. Wang, Y. Wang, Z.-N. Wang, P. Wappner, C. Ward, D.M. Ward, G. Warnes, H. Watada, Y. Watanabe, K. Watase, T.E. Weaver, C.D. Weekes, J. Wei, T. Weide, C.C. Weihl, G. Weindl, S.N. Weis, L. Wen, X. Wen, Y. Wen, B. Westermann, C.M. Weyand, A.R. White, E. White, J.L. Whitton, A.J. Whitworth, J. Wiels, F. Wild, M.E. Wildenberg, T. Wileman, D.S. Wilkinson, S. Wilkinson, D. Willbold, C. Williams, K. Williams, P.R. Williamson, K.F. Winklhofer, S.S. Witkin, S.E. Wohlgemuth, T. Wollert, E.J. Wolvetang, E. Wong, G.W. Wong, R.W. Wong, V.K.W. Wong, E.A. Woodcock, K.L. Wright, C. Wu, D. Wu, G.S. Wu, J. Wu, J. Wu, M. Wu, M. Wu, S. Wu, W.K. Wu, Y. Wu, Z. Wu, C.P. Xavier, R.J. Xavier, G.-X. Xia, T. Xia, W. Xia, Y. Xia, H. Xiao, J. Xiao, S. Xiao, W. Xiao, C.-M. Xie, Z. Xie, Z. Xie, M. Xilouri, Y. Xiong, C. Xu, C. Xu, F. Xu, H. Xu, H. Xu, J. Xu, J. Xu, J. Xu, L. Xu, X. Xu, Y. Xu, Y. Xu, Z.-X. Xu, Z. Xu, Y. Xue, T. Yamada, A. Yamamoto, K. Yamanaka, S. Yamashina, S. Yamashiro, B. Yan, B. Yan, X. Yan, Z. Yan, Y. Yanagi, D.-S. Yang, J.-M. Yang, L. Yang, M. Yang, P.-M. Yang, P. Yang, Q. Yang, W. Yang, W.Y. Yang, X. Yang, Y. Yang, Y. Yang, Z. Yang, Z. Yang, M.-C. Yao, P.J. Yao, X. Yao, Z. Yao, Z. Yao, L.S. Yasui, M. Ye, B. Yedvobnick, B. Yeganeh, E.S. Yeh, P.L. Yeyati, F. Yi, L. Yi, X.-M. Yin, C.K. Yip, Y.-M. Yoo, Y.H. Yoo, S.-Y. Yoon, K.-I. Yoshida, T. Yoshimori, K.H. Young, H. Yu, J.J. Yu, J.-T. Yu, J. Yu, L. Yu, W.H. Yu, X.-F. Yu, Z. Yu, J. Yuan, Z.-M. Yuan, B.Y. Yue, J. Yue, Z. Yue, D.N. Zacks, E. Zacksenhaus, N. Zaffaroni, T. Zaglia, Z. Zakeri, V. Zecchini, J. Zeng, M. Zeng, Q. Zeng, A.S. Zervos, D.D. Zhang, F. Zhang, G. Zhang, G.-C. Zhang, H. Zhang, H. Zhang, H. Zhang, H. Zhang, J. Zhang, J. Zhang, J. Zhang, J. Zhang, L. Zhang, L. Zhang, L. Zhang, M. Zhang, M.-Y. Zhang, X. Zhang, X.D. Zhang, Y. Zhang, Y. Zhang, Y. Zhang, Y. Zhang, Y. Zhang, M. Zhao, W.-L. Zhao, X. Zhao, Y.G. Zhao, Y. Zhao, Y. Zhao, Y. Zhao, Z. Zhao, Z.J. Zhao, D. Zheng, X.-L. Zheng, X. Zheng, B. Zhivotovsky, Q. Zhong, G.-Z. Zhou, G. Zhou, H. Zhou, S.-F. Zhou, X. Zhou, H. Zhu, H. Zhu, W.-G. Zhu, W. Zhu, X.-F. Zhu, Y. Zhu, S.-M. Zhuang, X. Zhuang, E. Ziparo, C.E. Zois, T. Zoladek, W.-X. Zong, A. Zorzano, S.M. Zughaier, Guidelines for the use and interpretation of assays for monitoring autophagy (3rd edition), Autophagy 12 (2016) 1–222, http://dx.doi.org/10.1080/15548627.2015.1100356.

[23] A. Höhn, T. Jung, S. Grimm, T. Grune, Lipofuscin-bound iron is a major intracellular source of oxidants: role in senescent cells, Free Radic. Biol. Med. 48 (2010) 1100–1108, http://dx.doi.org/10.1016/j.freeradbiomed.2010.01.030.

[24] G.P. Dimri, X.H. Lee, G. Basile, M. Acosta, C. Scott, C. Roskelley, E.E. Medrano, M. Linskens, I. Rubelj, O. Pereirasmith, M. Peacocke, J. Campisi, A biomarker that

identifies senescent human-cells in culture and in aging skin in-vivo, Proc. Natl. Acad. Sci. U. S. A. 92 (1995) 9363–9367.
[25] E.C. Filippi-Chiela, M.M. Oliveira, B. Jurkovski, S.M. Callegari-Jacques, V.D. da Silva, G. Lenz, Nuclear morphometric analysis (NMA): screening of senescence, apoptosis and nuclear irregularities, PLoS One 7 (2012), e42522 http://dx.doi.org/10.1371/journal.pone.0042522.
[26] A. Terman, U.T. Brunk, Aging as a catabolic malfunction, Int. J. Biochem. Cell Biol. 36 (2004) 2365–2375, http://dx.doi.org/10.1016/j.biocel.2004.03.009.
[27] C.a. Schonewolf, M. Mehta, D. Schiff, H. Wu, B.G. Haffty, V. Karantza, S.K. Jabbour, Autophagy inhibition by chloroquine sensitizes HT-29 colorectal cancer cells to concurrent chemoradiation, World J. Gastrointest. Oncol. 6 (2014) 74–82, http://dx.doi.org/10.4251/wjgo.v6.i3.74.
[28] D.C. Rubinsztein, A.M. Cuervo, B. Ravikumar, S. Sarkar, V. Korolchuk, S. Kaushik, D.J. Klionsky, In search of an "autophagomometer", Autophagy 5 (2009) 585–589, http://dx.doi.org/10.4161/auto.5.5.8823.
[29] L. Potze, S. Di Franco, C. Grandela, M.L. Pras-Raves, D.I. Picavet, H.a. van Veen, H. van Lenthe, F.B. Mullauer, N.N. van der Wel, A. Luyf, a.H.C. van Kampen, S. Kemp, V. Everts, J.H. Kessler, F.M. Vaz, J.P. Medema, Betulinic acid induces a novel cell death pathway that depends on cardiolipin modification, Oncogene (2015) 1–11, http://dx.doi.org/10.1038/onc.2015.102.
[30] Y. Chen, R. Sun, B. Wang, Monolayer behavior of binary systems of betulinic acid and cardiolipin: thermodynamic analyses of Langmuir monolayers and AFM study of Langmuir-Blodgett monolayers, J. Colloid Interface Sci. 353 (2011) 294–300, http://dx.doi.org/10.1016/j.jcis.2010.09.019.
[31] M. Gao, P.M. Lau, S.K. Kong, Mitochondrial toxin betulinic acid induces in vitro eryptosis in human red blood cells through membrane permeabilization, Arch. Toxicol. 88 (2014) 755–768, http://dx.doi.org/10.1007/s00204-013-1162-x.
[32] W.X. Ding, H.M. Ni, M. Li, Y. Liao, X. Chen, D.B. Stolz, G.W. Dorn, X.M. Yin, Nix is critical to two distinct phases of mitophagy, reactive oxygen species-mediated autophagy induction and Parkin-ubiquitin-p62-mediated mitochondrial priming, J. Biol. Chem. 285 (2010) 27879–27890, http://dx.doi.org/10.1074/jbc.M110.119537.
[33] A. Terman, H. Dalen, J.W. Eaton, J. Neuzil, U.T. Brunk, Aging of cardiac myocytes in culture: oxidative stress, lipofuscin accumulation, and mitochondrial turnover, Ann. N. Y. Acad. Sci. (2004) 70–77, http://dx.doi.org/10.1196/annals.1297.015.
[34] C.-H. Wang, S.-B. Wu, Y.-T. Wu, Y.-H. Wei, Oxidative stress response elicited by mitochondrial dysfunction: implication in the pathophysiology of aging, Exp. Biol. Med. (Maywood) 238 (2013) 450–460, http://dx.doi.org/10.1177/1535370213493069.
[35] A. Höhn, T. Grune, Lipofuscin: formation, effects and role of macroautophagy, Redox Biol. 1 (2013) 140–144, http://dx.doi.org/10.1016/j.redox.2013.01.006.
[36] U.T. Brunk, A. Terman, Lipofuscin: mechanisms of age-related accumulation and influence on cell function, Free Radic. Biol. Med. 33 (2002) 611–619.
[37] U.T. Brunk, A. Terman, The mitochondrial-lysosomal axis theory of aging: accumulation of damaged mitochondria as a result of imperfect autophagocytosis, Eur. J. Biochem. 269 (2002) 1996–2002, http://dx.doi.org/10.1046/j.1432-1033.2002.02869.x.
[38] K. Bayreuther, H.P. Rodemann, R. Hommel, K. Dittmann, M. Albiez, P.I. Francz, Human skin fibroblasts in vitro differentiate along a terminal cell lineage, Proc. Natl. Acad. Sci. U. S. A. 85 (1988) 5112–5116, http://dx.doi.org/10.1073/pnas.85.14.5112.
[39] R. Salama, M. Sadaie, M. Hoare, M. Narita, Cellular senescence and its effector programs, Genes Dev. 28 (2014) 99–114, http://dx.doi.org/10.1101/gad.235184.113.
[40] Z. Mao, Z. Ke, V. Gorbunova, A. Seluanov, Replicatively senescent cells are arrested in G1 and G2 phases, Aging (Albany NY) 4 (2012) 431–435.
[41] W. Ma, C. Hommel, P. Brenneisen, T. Peters, N. Smit, J. Sedivy, K. Scharffetter-Kochanek, M. Wlaschek, Long-term growth arrest of PUVA-treated fibroblasts in G2/M in the absence of p16(INK4a) p21(ClP1) or p53, Exp. Dermatol. 12 (2003) 629–637.
[42] A.R.J. Young, M. Narita, M. Ferreira, K. Kirschner, M. Sadaie, J.F.J. Darot, S. Tavaré, S. Arakawa, S. Shimizu, F.M. Watt, M. Narita, Autophagy mediates the mitotic senescence transition, Genes Dev. 23 (2009) 798–803, http://dx.doi.org/10.1101/gad.519709.
[43] M.T. Villanueva, DNA repair: a new tool to target DNA repair, Nat. Rev. Cancer 15 (2015) 136, http://dx.doi.org/10.1038/nrc3919.
[44] R. Csuk, Betulinic acid and its derivatives: a patent review (2008 – 2013), Expert Opin. Ther. Pat. 24 (2014) 913–923, http://dx.doi.org/10.1517/13543776.2014.927441.